Ore Geology Reviews 90 (2017) 65–93

Contents lists available at ScienceDirect

Ore Geology Reviews

journal homepage: www.elsevier.com/locate/oregeo

The significance of magmatic erosion for bifurcation of UG1 chromitite layers in the Bushveld Complex

Mosili Pebane [a], Rais Latypov [b,*]

[a] Mineralogy Division, Mintek, Randburg, South Africa
[b] School of Geosciences, University of the Witwatersrand, Johannesburg, South Africa

ARTICLE INFO

Article history:
Received 16 June 2016
Received in revised form 3 February 2017
Accepted 9 February 2017
Available online 24 February 2017

Keywords:
Bifurcating chromitite layers
Bushveld Complex
Basal magma layers
Superheated magma
Magmatic erosion
In situ crystallization
Multiple emplacement
Convection
Cumulates
Layered intrusions
South Africa

ABSTRACT

One of the most puzzling features of the UG1 chromitite layers in the famous exposures at Dwars River, Eastern Bushveld Complex, is the bifurcation, i.e. convergence and divergence of layers along strike that isolate lenses of anorthosite. The bifurcations have been variously interpreted as resulting from: (1) the intermittent accumulation of plagioclase on the chamber floor as lenses, terminated by crystallization of continuous chromitite layers (the depositional model); (2) late-stage injections of chromite mush or chromite-saturated melt along anastomosing fractures that dismembered semi-consolidated plagioclase cumulates (the intrusive model); (3) post-depositional deformation of alternating plagioclase and chromite cumulates, resulting in local amalgamation of chromitite layers and anorthosite lenses that wedge out laterally (the deformational model). None of these hypotheses account satisfactorily for the following field observations: (a) wavy and scalloped contacts between anorthosite and chromitite layers; (b) abrupt lateral terminations of thin anorthosite layers within chromitite; (c) *in situ* anorthosite inclusions with highly irregular contacts and delicate wispy tails within chromitite; many of these inclusions are contiguous with footwall and hanging wall cumulates; (d) transported anorthosite fragments enclosed by chromitite; (e) disrupted anorthosite and chromitite layers overlain by planar chromitite; (f) protrusions of chromitite into underlying anorthosite; (g) merging of chromitite layers around anorthosite domes. We propose a novel hypothesis that envisages basal flows of new dense and superheated magma that resulted in intense thermo-chemical erosion of the temporary floor of the chamber. The melting and dissolution of anorthosite was patchy and commonly inhibited by chromitite layers, resulting in lens-like remnants of anorthosite resting on continuous layers of chromitite. On cooling, the magma crystallized chromite on the irregular chamber floor, draping the remnants of anorthosite and merging with pre-existing chromitite layers excavated by erosion. With further cooling, the magma crystallized chromite-bearing anorthosite. Emplacement of multiple pulses of magma led to repetition of this sequence of events, resulting in a complex package of anorthosite lenses and bifurcating chromitite layers. This hypothesis is the most satisfactory explanation for most of the features of this enigmatic igneous layering in the Bushveld Complex.

1. Introduction

Modal layering is one of the most spectacular features in intrusive igneous bodies of various compositions. The most extreme examples of this phenomenon are generally found in mafic-ultramafic intrusions. A plethora of mechanisms has been proposed for different types of igneous layering in these intrusions. These encompass a wide range of dynamic processes such as gravity settling of crystals, flow segregation in crystal-laden magmas, magma injection as plumes or as basal flows, mineral re-orientation, hydrodynamic sorting of minerals and magmatic deformation (e.g. Naslund and McBirney, 1996; Namur et al., 2015). Other hypotheses involve non-dynamic processes such as ephemeral changes in pressure, temperature and oxygen fugacity or variations in nucleation and growth rates (e.g. Naslund and McBirney, 1996; Namur et al., 2015). It has become increasingly clear that layering can be produced by distinctly different processes, even within the same plutonic body (Namur et al., 2015), suggesting that each type of layering should be interpreted based on its own unique characteristics.

In this paper we revisit enigmatic igneous layering within predominately anorthositic cumulates underlying the Upper Group (UG) 1 stratiform chromitite layer in the Bushveld Igneous

* Corresponding author.
E-mail address: rais.latypov@wits.ac.za (R. Latypov).

http://dx.doi.org/10.1016/j.oregeorev.2017.02.026
0169-1368/

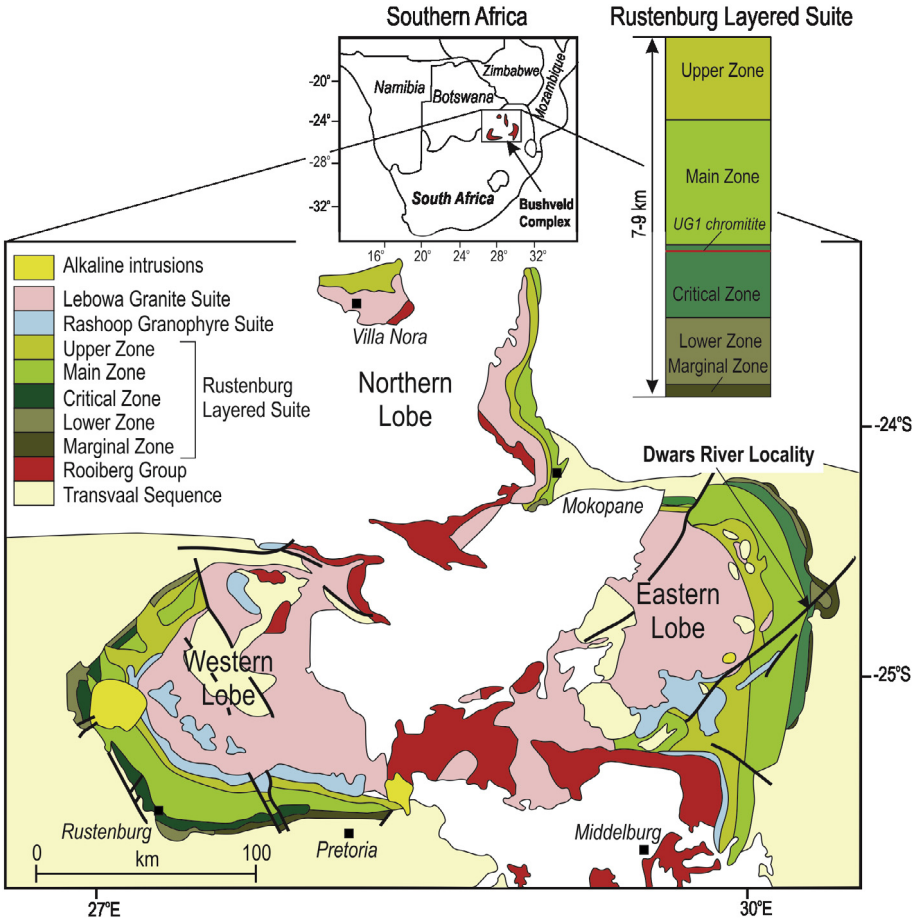

Fig. 1. Location and simplified geological map of the Bushveld Igneous Complex (Rustenburg Layered Suite) indicating the location of the Dwars River Locality (DRL). The stratigraphic column shows the position of the UG1 chromitite near the top of the Critical Zone. The map is modified after Webb (2009).

Complex (BIC). It is well exposed at the Dwars River Locality (DRL) of the Eastern Bushveld (Fig. 1), for this reason designated a National Monument. The UG1 chromitite is an up to 2 m thick massive layer overlying a sequence of thinner chromitite layers hosted in the footwall anorthosite (Fig. 2A). The chromitite layers within anorthosite show numerous examples of bifurcations, a feature characterised by both upward and downward branching of thin chromitite layers that continue on from a single, thicker chromitite layer (Fig. 3). It should be noted that bifurcation is not a unique feature to UG1 chromitites. Localised examples of bifurcation have been reported in the UG2 and LG5 chromitites of the BIC (e.g. Cousins and Feringa, 1964; Schürmann et al., 1998) and may in fact be common for most chromitite layers hosted by orthopyroxenite (e.g. Cawthorn, 2015). However, the bifurcation of UG1 chromitites within anorthosite is by far the most eye-catching and has inspired many researchers to attempt to explain the phenomenon (e.g. Van Biljon, 1963; Ferguson and Botha, 1963; Wager and Brown, 1967; Lee, 1981; De Klerk, 1992; Nex, 2004; Maier and Barnes, 2008; Voordouw et al., 2009; Maier et al., 2013; Cawthorn, 2003, 2015), but it still remains largely unresolved. It is noteworthy that some features of the chromitite-anorthosite layering are so similar to those observed in sedimentary rocks that some researchers have even suggested that the layering at the DRL was the result of the metasomatic transformation of beds of chert and limestone (e.g. Van Biljon, 1963). The diverse opinions on the origin of the layering was recognised by Wager and Brown (1967, p. 363) who noted that suggestions have included 'both that chromitite liquids have intruded anorthosite layers and that anorthosite liquids have intruded chromitite layers'. It is surprising and perhaps disturbing, that the field relations remain as puzzling as they did half a century ago.

We approach this petrological enigma by focusing on detailed field relationships that appear to be the most important constraints on the dynamic magmatic processes involved in the formation of the layering. One of our aims is to emphasize that, apart from the principal type of UG1 chromitite bifurcation, there are three additional subtypes, which are likely produced by distinctly different processes. This may be one of the reasons why previous attempts to explain this phenomenon by one specific process were not particularly successful. Our most important aim is to demonstrate that the field relationships provide convincing evidence for the crucial role of *magmatic erosion* in the origin of the principal type of UG1 chromitite bifurcations, a process seldom considered as a realistic agent in the formation of igneous layering (e.g. Naslund and McBirney, 1996; Namur et al., 2015). This inference is in line with the current consensus among many Bushveld petrologists that magmatic erosion played an important role in several petrological aspects of the complex (e.g. Vermaak, 1976; Kruger and Marsh, 1985; Campbell, 1986; Eales et al., 1988; Smith et al., 2003; Cawthorn et al., 2005; Roberts et al., 2007; Naldrett et al., 2011; Latypov et al., 2015, 2017; Mukherjee et al., 2017).

2. The Bushveld Complex and its chromitite layers

The Bushveld Complex is a ~2056 Ma (Zeh et al., 2015) world-renowned Platinum Group Element (PGE) repository that has been described in many publications (e.g. Eales and Cawthorn, 1996;

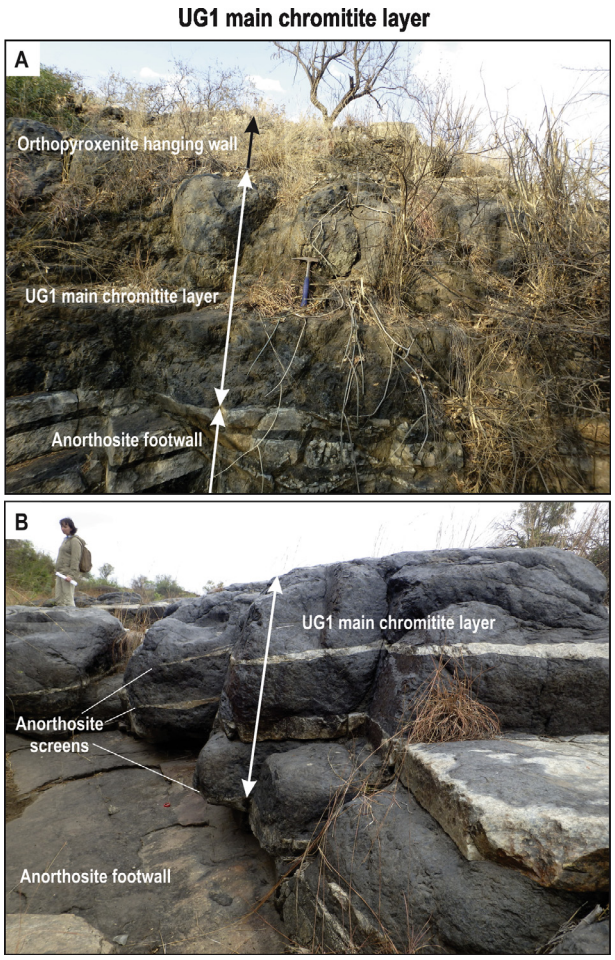

Fig. 2. Photographs of the main UG1 chromitite. (A) UG1 chromitite (180 cm thick) underlain by anorthosite with thin chromitite layers and overlain by orthopyroxenite with thin anorthosite layers. (B) UG1 chromitite comprising several sublayers separated by tapering anorthosite screens. GPS coordinates: (A) point 334, latitude −24.911658° and longitude 30.103252°; (B) point 364, latitude −24.910583° and longitude 30.103387°.

Maier and Barnes, 1999; Kinnaird et al., 2002; Mondal and Mathez, 2007; Naldrett et al., 2012; Cawthorn, 2015). It is also the largest known mafic-ultramafic plutonic intrusion in the world. It occupies an area of more than 90000 km^2 and extends ~430 km East-West and ~300 km North-South (Naldrett et al., 2009; Eales and Costin, 2012; Finn et al., 2015). It is a discontinuous oval body consisting of five major lobes: the Northern, Western, Far Western, Eastern and South-Eastern (Fig. 1; Cawthorn and Walraven, 1998; Kinnaird et al., 2002). The BIC comprises volcanic roof rocks (the Rooiberg Group), a 7–9 km thick sequence of ultramafic to mafic rocks of the Rustenburg Layered Suite (RLS), the Rashoop Granophyre Suite and the granites of the Lebowa Granite Suite. The RLS is further divided into the Marginal, Lower, Critical, Main and Upper zones on the basis of different cumulus assemblages (Hall, 1932). Central to this work are the stratiform chromitites of the BIC, which are persistent over hundreds of kilometres. Stratiform chromitites in the RLS are subdivided into the Lower Group chromitites (LG1-7), Middle Group chromitites (MG1-4) and Upper Group chromitites (UG). The latter comprise the UG1 and 2 layers as well as the UG3 layer present in the Eastern Bushveld (e.g. Cousins and Feringa, 1964; Scoon and Teigler, 1994; Teigler and Eales, 1996). LG chromitites are generally hosted by feldspathic orthopyroxenite and attain an aggregate thickness of ~3.5 m. The LG1-4 chromitites are unique in that they are olivine-rich, whereas overlying chromitite layers commonly lack olivine (Hatton and von Gruenewaldt, 1987). The MG chromitites together attain a thickness of ~4 m and are typically hosted within pyroxenite and norite. The UG chromitites have individual thicknesses of about 1 m and they are typically enclosed by anorthosite or orthopyroxenite (Gain, 1985; Hatton and von Gruenewaldt, 1987).

3. Field relations of the primary igneous layering

This study is principally based on observations from the DRL in the Eastern Bushveld Complex (Fig. 1). Here, chromitite and anorthosite layers can be locally examined in 3D, which is rarely possible in underground exposures. We provide GPS coordinates of all featured outcrops in the figure captions and the separate KML file in the electronic attachment. The main UG1 chromitite layer at the DRL is 170–180 cm thick and it is accompanied by several millimetres to decimetre thick UG1 sublayers within the footwall anorthosite (Fig. 2A). It is overlain here by a sequence of predominantly orthopyroxenite and norite that includes a few layers of anorthosite. Along strike, the main UG1 layer is not everywhere massive but is locally split into several thinner sublayers by screens of anorthosite that generally wedge out along strike (Fig 2B). Locally, where the screens disappear, the main UG1 layer is entirely massive. Only the lowermost 60 cm of the main UG1 layer is preserved beside the extensive flat surfaces of the outcrop (Fig. 3A). The interlayered chromitite and anorthosite produce the distinctive 'zebra-type layering' for which this locality is well known (Fig. 3). The footwall and hanging wall rocks to this sequence are orthopyroxenite/norite but they are poorly-exposed at this locality (Nex, 2004). We have subdivided all our field observations into two major groups. The first comprises various features of chromitite-anorthosite layers that appear to have become established during formation at the magmatic stage. These can be referred to as primary cumulus features. The second includes various features that are related to the modification, deformation and disruption of pre-existing chromitite and anorthosite layers. These can be referred to as postcumulus features. The most important primary cumulus features of chromitite-anorthosite layers identified during this study are summarized below.

3.1. Bifurcations of chromitite layers

The anastomosing chromitites are characterised by the lateral splitting of a single chromitite layer into two or more thinner chromitites (Fig. 3). These thinner layers or lamina may re-join a few centimetres to several metres along strike, isolating lenses of anorthosite (in cross-section). The 3D shape of these "lenses" is not yet properly documented but likely represents sub-circular discs or elongated pillows. Importantly, the lenses between bifurcating chromitite layers are the principal reason for the splitting and merging of the layers along the strike and constitute the most fundamental features of this layering. The total thickness of chromitite branches is always close to that of the single chromitite layer from which these layers diverge from or merge into (e.g. Ferguson and Botha, 1963; Cawthorn, 2003). Although it has been argued that on a large scale the splitting of chromitite layers may have a preferred direction (e.g. Nex, 2004), chromitite layers commonly bifurcate in opposite directions within small areas (Fig. 3B–C). In consequence, bifurcations are commonly accompanied by chromitite layers apparently bridging different stratigraphic horizons (Fig. 3B–C). This appears to be a unique feature of the layering and has not been documented elsewhere (e.g. Naslund and McBirney, 1996; Namur et al., 2015). The anorthosite between chromitites is "mottled" i.e. characterised by the presence

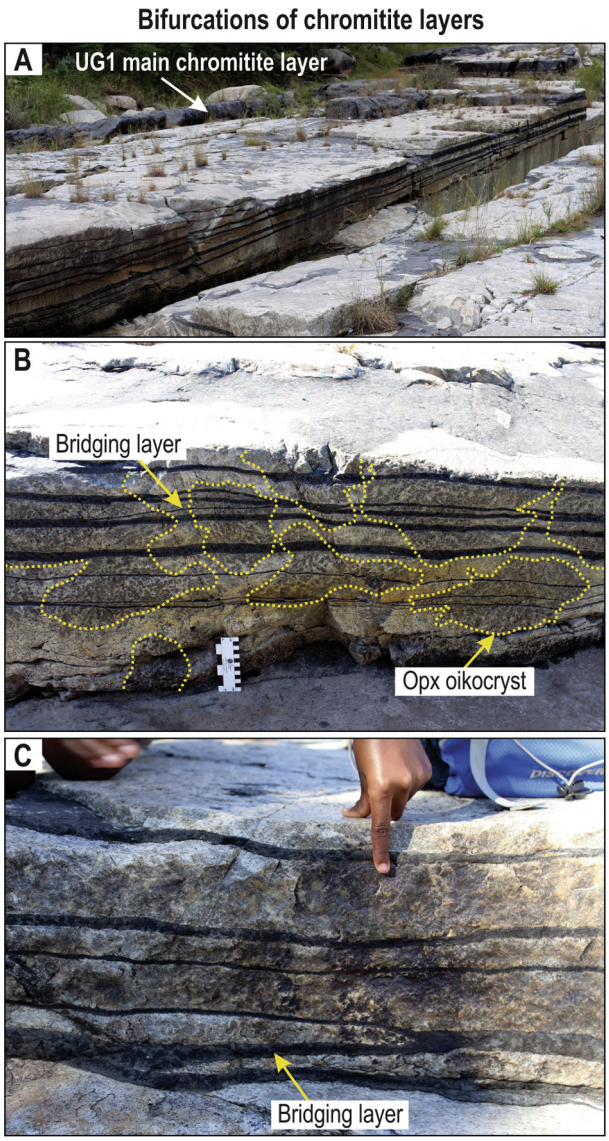

Fig. 3. Photographs of chromitite-anorthosite layering. (A) Chromitite and anorthosite layers with chromitite layers generally bifurcating from the top-right corner to the bottom-left corner of the picture over several tens of metres. (B) and (C) Chromitite layers bifurcating over a distance of several decimetres. Note chromitite layers in (B) and (C) that bridge different stratigraphic horizons. Large orthopyroxene oikocrysts are clearly visible in anorthosite and superficially appear to be crosscut by the UG1 chromitite seams in B. GPS coordinates: (A) point 357, latitude −24.910764° and longitude 30.103325°; (B) point 341, latitude −24.911038° and longitude 30.103194°; (C) point 343, latitude −24.911016° and longitude 30.103226°.

of decimetre-wide orthopyroxene oikocrysts that superficially appear to be cross-cut by chromitite layers (Fig. 3B, but see below).

3.2. Contacts and disintegration of basal anorthosite

Most contacts between chromitite and anorthosite layers are sharp and planar (Fig. 3). There are, however, some uneven and gradational contacts as well (Fig. 4). Some wavy contacts persist laterally over several metres. They occur between chromitite and both hanging wall (Fig. 4A–C) and footwall (Fig. 4D) anorthosite. Contacts are particularly uneven in places where the footwall anorthosite shows signs of disintegration into small inclusions (Fig. 5A), most of them touching each other and some being apparently still attached to the footwall anorthosite (Fig. 5B). In some instances, the chromitite layers, especially at their bases, contain numerous small anorthosite inclusions which locally occupy up to 50% of the volume. It is conceivable that most, if not all, of these inclusions are connected in three dimensions.

3.3. Lateral termination of anorthosite layers within chromitite

Thin anorthosite layers within massive chromitite pinch out in places and re-appear along strike (Fig. 6). Cm- to dm-long gaps separate anorthosite lenses that lie at the same stratigraphic horizon suggesting that they were originally continuous anorthosite layers (Fig. 6A). Significantly, tapering and termination of anorthosite layers results in merging of separate chromitite sublayers into a single thicker layer of chromitite (Fig. 6B). This is also a feature of the UG1 main layer (Fig. 2B). The chromitite sublayers terminate gradually as thin anorthosite layers give way to millimetre-wide tails of *in situ* anorthosite inclusions. Note that the anorthosite lenses in this outcrop exhibit lobate contacts with underlying chromitite but planar contacts with the overlying chromitite (Fig. 6A, C).

3.4. In situ anorthosite inclusions within chromitite

Anorthosite inclusions that are inferred to be related to the lateral termination of anorthosite layers are quite common in some chromitite layers. These *in situ* inclusions range in size from several millimetres to tens of centimetres (Fig 7). They are typically elongate and terminate into wispy tails (Fig. 7A–B). Inclusions exhibit planar (Fig. 7B) or irregular (Fig. 7C) contacts with the surrounding chromitite. Locally, small protrusions (fingers) of chromitite are present in anorthosite inclusions (Fig. 7D). In places the protrusions continue in the inclusions as millimetre thick veins of chromitite (Fig. 7D).

3.5. Transported blocks of anorthosite within chromitite

There are examples of sub-rounded to angular centimetre-wide anorthosite inclusions within some chromitite layers. They have probably been transported from an external source (Fig. 8). Significantly, the total thickness of the chromitite seams above and below these blocks is less than the thickness of the adjacent chromitite layers. This is not the case in of bifurcating chromitite layers (Fig. 3). More importantly, the chromitite layer contacts are deflected around some anorthosite blocks (Fig. 8).

3.6. Non-deformed and continuous chromitite layers overlying disrupted layered sequences

One common feature of localities with deformed and displaced chromitite layers is that they are overlain by continuous chromitite layers (Fig. 9A–C). The continuous chromitite layers show no evidence of deformation: they are neither disrupted nor do they preserve evidence of significant displacement in any direction. Importantly, not only single chromitite layers but also bifurcating layers are displaced by faults in places (e.g. Fig. 9A).

3.7. Lateral protrusions of chromitite into footwall anorthosite

In places, there are sill-like protrusions of chromitite in underlying anorthosite. The clearest example of this is a ~7 cm thick body (Fig. 10) that branches from the UG1 main chromitite layer into its footwall. The protrusion extends laterally for about 30 cm (Fig. 10 A, C) and locally has an intricate contact with the overlying screen of anorthosite (Fig. 10E). In close proximity to the chromitite protrusion there is a rectangular anorthosite block apparently suspended in chromitite (Fig. 10 A, B). A closer examination of this

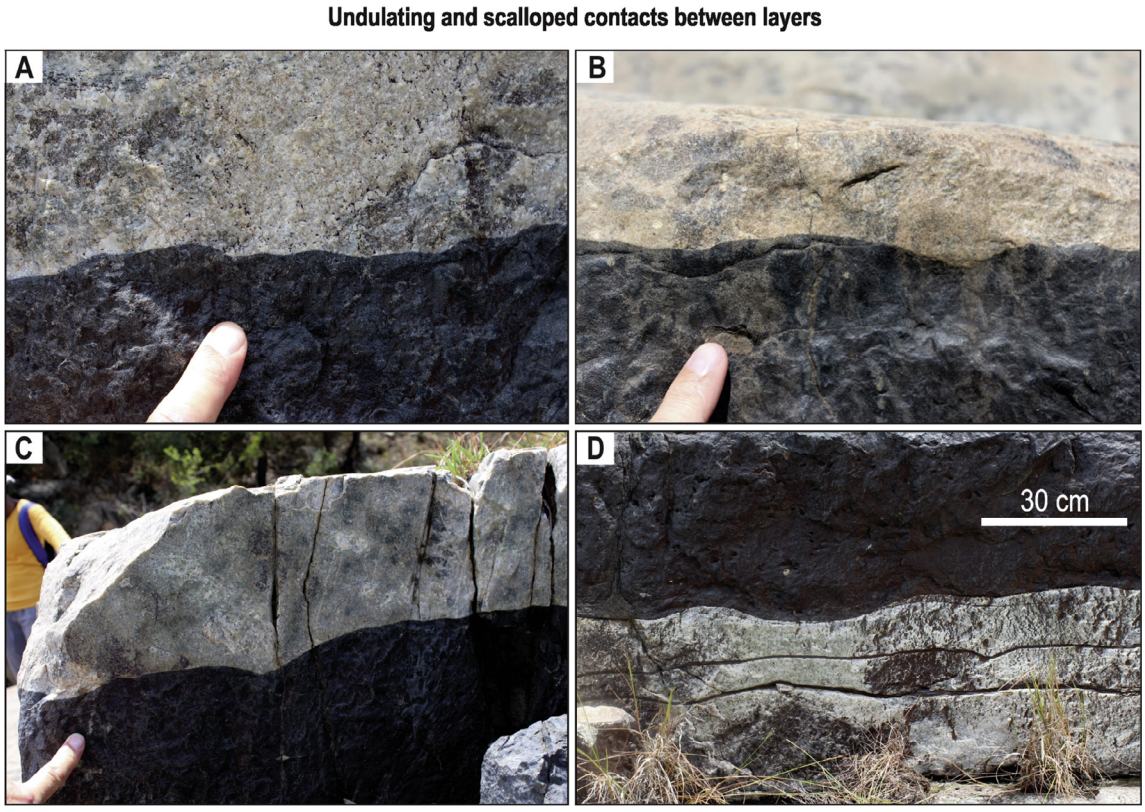

Fig. 4. Photographs of undulating and scalloped contacts between chromitite (black) and overlying anorthosite (white) in (A), (B) and (C) and between anorthosite and overlying chromitite in (D). GPS coordinates: (A) point 367, latitude −24.91048° and longitude 30.103446°; (B) point 362, latitude −24.910664° and longitude 30.10343°; (C) point 366, latitude −24.910498° and longitude 30.103472°; (D) point 354, latitude −24.910843° and longitude 30.103207°.

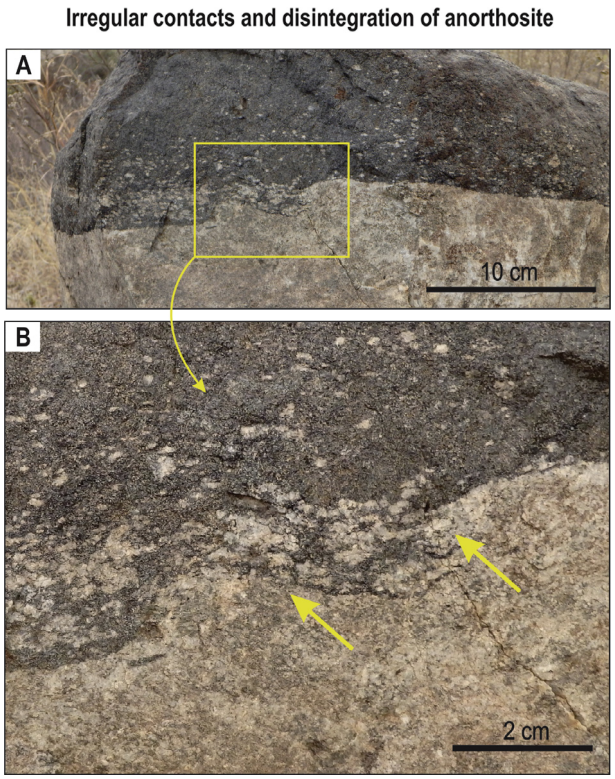

Fig. 5. Photographs of the upper contact of footwall anorthosite (A) that is uneven because of the disintegration of the anorthosite into small inclusions, some of which are still partly attached to the footwall (B, indicated by arrows). GPS coordinates: point 376, latitude −24.909623° and longitude 30.104038°.

anorthosite block reveals uneven contacts with the host chromitite. Interesting, the shape of the lower contact of the anorthosite block closely matches that of the upper contact of the underlying anorthosite like two pieces of a jigsaw puzzle (Fig. 10D). Another informative outcrop shows several chromitite seams that extend from a thicker chromitite layer into its footwall anorthosite (Fig. 11A). The lower part of the thick layer and protrusions themselves contain numerous small anorthosite inclusions which locally occupy up to 30–50% of the rock's volume. Some of these inclusions along both margins of chromitite protrusions are partly attached to the host anorthosite resulting in extremely uneven contacts and indicating that the inclusions are autoliths (Fig. 11B, black arrows) produced by the *in situ* disintegration of anorthosite (see also Fig. 5). In some places the chromitite seams are almost choked with anorthosite inclusions (Fig. 11C–F), some of which remain connected to footwall and hanging wall anorthosite. This indicates that the source of these and most other neighbouring inclusions was the adjacent anorthosite and that transport of these inclusions from their source was small. Note also that the thicknesses of the chromitite protrusions vary substantially over a few cm; their upper and lower contacts are non-parallel and uneven (Fig. 11, C-F).

3.8. Composite chromitite layers

There are composite layers of chromitite that are composed of several sublayers with distinctly different contents of small anorthosite inclusions and with quite sharp boundaries between them. Fig. 12 illustrates one example of such a composite chromitite layer that consists of two juxtaposed sublayers of different composition: the thicker uppermost layer is a massive coarse-grained chromitite with some large anorthosite autoliths and the

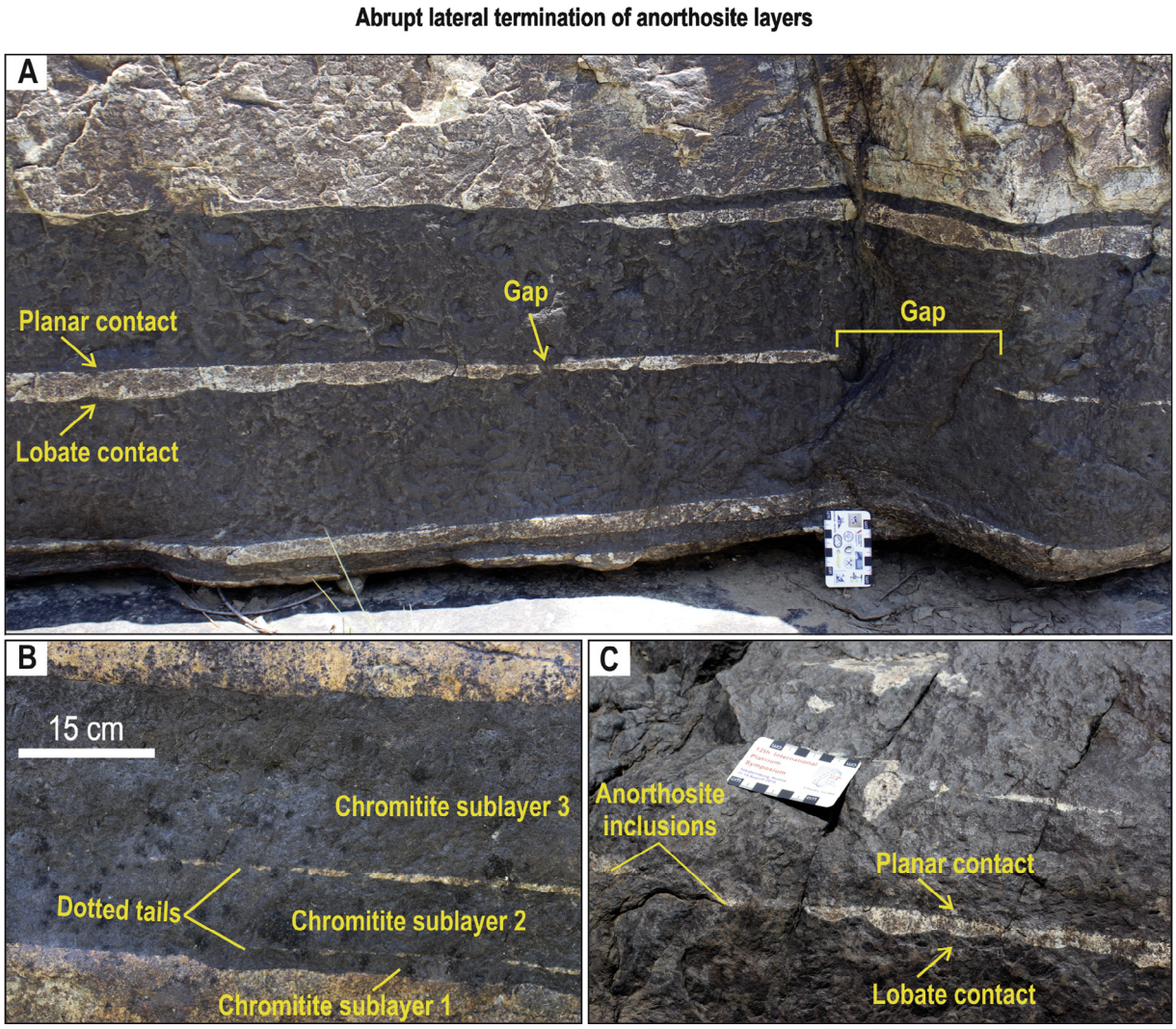

Fig. 6. Photographs of anorthosite layers and lenses that thin and wedge out laterally in massive chromitites. (A) Anorthosite layer with a lobate contact with underlying chromitite and a 1 cm-wide gap between adjacent lenses and a 10 cm gap which terminates in a discontinuous tail at the same stratigraphic horizon. (B) Two anorthosite lenses terminating into millimetre-thick discontinuous tails which results in merging of three chromitite sublayers into a single, thicker chromitite. (C) Anorthosite layer with a planar upper contact and scalloped lower contact with isolated anorthosite inclusions at the same horizon. GPS coordinates for (A), (B) and (C): point 361, latitude −24.910647° and longitude 30.103424°.

thinner lowermost one is a finer-grained chromitite with numerous small anorthosite inclusions. Note that there is no evidence of *in situ* disintegration of footwall anorthosite in this case (compare with Fig. 5). Chromitite layers containing abundant anorthosite inclusions may also occur in the central parts of the thicker chromitite layers. The inclusions in such layers cannot be *in situ* (because no anorthosite occurs directly below them) and must therefore be derived from somewhere else, transported along the floor of the magma chamber for some distance and then re-deposited in these layers.

4. Field relations of the disturbed igneous layering

4.1. Anorthosite domes and associated deformation

Nex (2004) described several domal structures at the DRL which he attributed to periodic extrusion of a plagioclase-rich mush on the chamber floor (see further description below). The photographs in Fig. 13 were taken from the margin of one of these structures that is accompanied by the abrupt truncation of all chromitite layers in the footwall anorthosite. In addition, some chromitite layers appear to have been deformed around the margins of the domes (Figs. 13A and 14A). The deformation is also obvious from comparison of two groups of subparallel chromitite layers with distinctly different dips (0, 1 and 2 versus 3, 4 and 5 in Fig. 13A). Layers 3, 4 and 5 are almost horizontal about two metres away from the margin of the domes whereas layers 0, 1 and 2 closer to the dome have a dip of about 45 degrees (Fig. 13A–B). The different orientation of the chromitite layers is unlikely to be primary and can be best explained by more intense deformation of layers 0, 1 and 2 that resulted in their merging with of the overlying layers at the margin of the domal structure (indicated by two arrows in Fig. 13B). Similar merging of chromitite layers at the margins of the dome is also seen in Fig. 13C (indicated by four arrows).

4.2. Plastic deformation and boudinage of chromitite layers

Plastic deformation of thin chromitite layers is particularly evident in the vicinity of anorthosite domes (Fig. 14). Some layers of chromitite are folded but still retain their continuity (Fig. 14A–B). Examples of more severe plastic deformation are characterised by folded and dismembered chromitites within anorthosite (Fig. 14C–D). However, despite being stretched and separated,

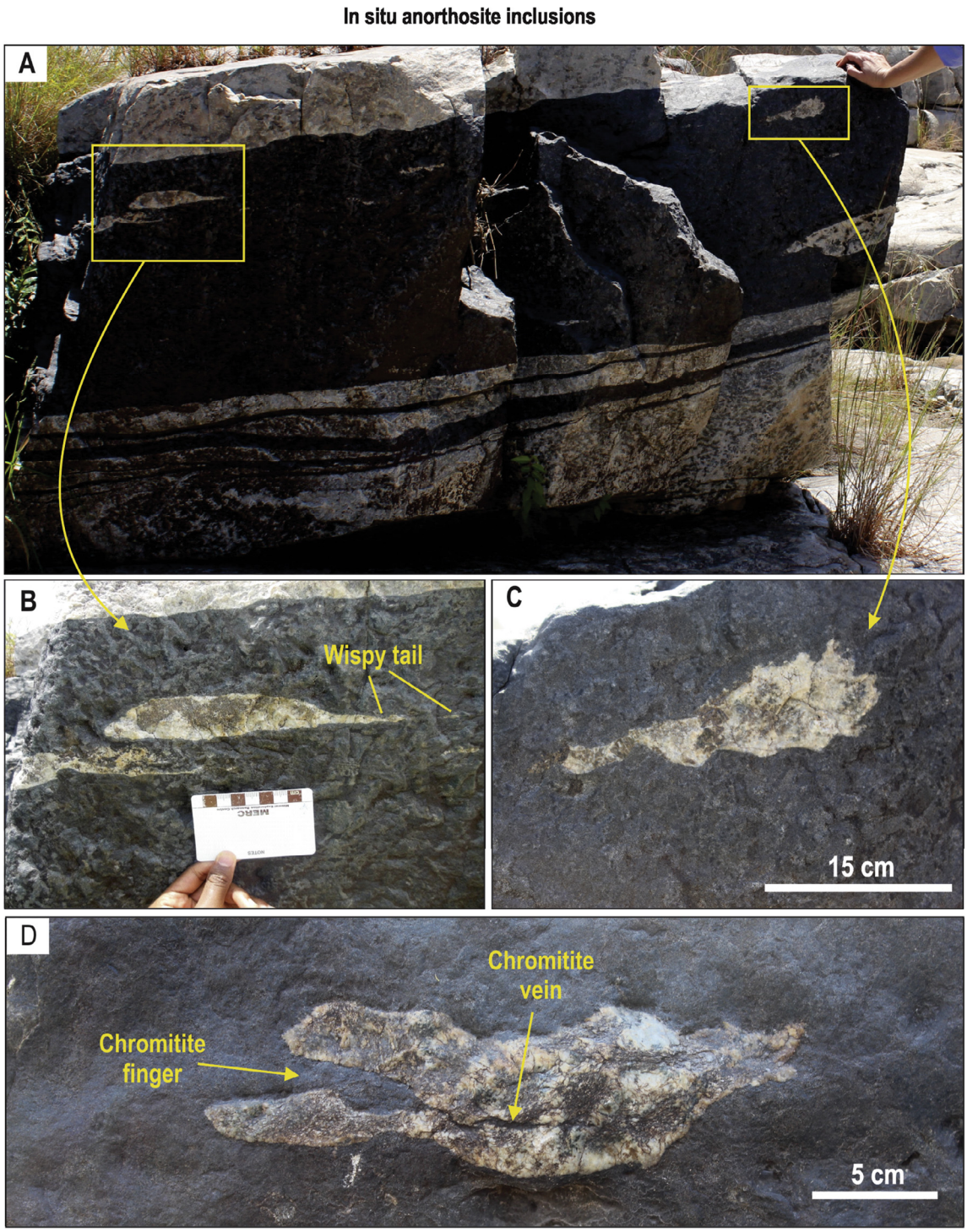

Fig. 7. Photographs of anorthosite inclusions in chromitite. (A) Bifurcating chromitite stringers overlain by the UG1 main layer that hosts anorthosite inclusions. (B) An elongated anorthosite inclusion that terminates in a thin, wispy and discontinuous tail. (C) An elongated anorthosite inclusion with scalloped contacts. (D) An elongated anorthosite inclusion with scalloped contacts and a chromitite finger protruding into its interior. GPS coordinates for (A), (B) and (C): point 366, latitude −24.910498° and longitude 30.103472°; (D) point 358, latitude −24.910657° and longitude 30.103273°.

individual chromitite layers still retain their individual integrity, indicating that these layers were almost consolidated prior to deformation. Some deformed chromitite layers are overlain by continuous, almost planar and apparently non-deformed chromitites (Fig. 14B; see also Fig. 9). In addition, some chromitite layers appear to have been locally subjected to stretching and boudinage (Fig. 15).

4.3. Brittle deformation of chromitite layers

Evidence of brittle deformation of thin chromitites interlayered with anorthosite is very common (Fig. 16). In places, chromitite layers are broken up and isolated in anorthosite. In cross-section, disrupted pieces of chromitite may remain in their original positions (Fig. 16B) or be displaced (Fig. 16C). These relations show

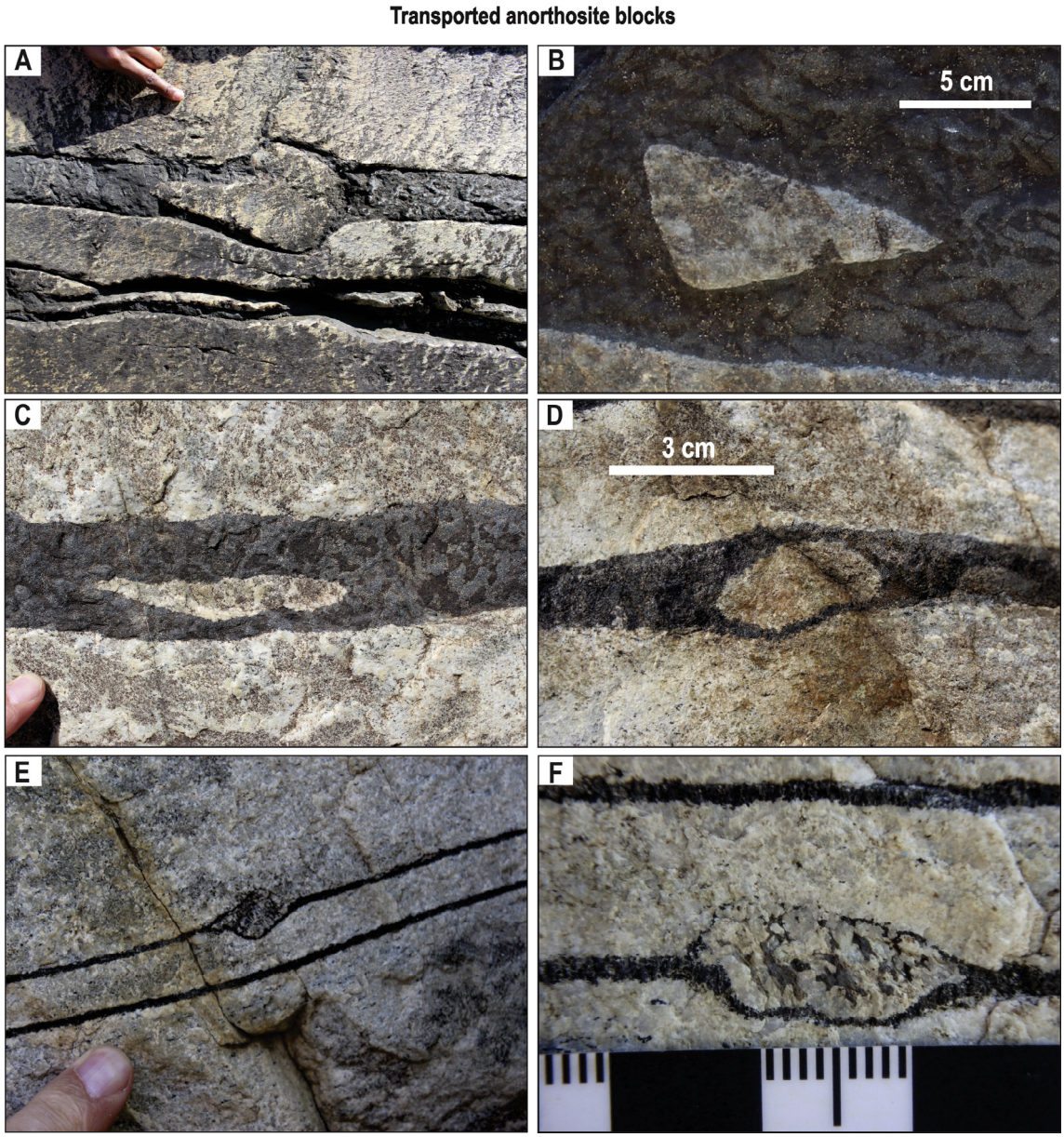

Fig. 8. Photographs of anorthosite blocks (A-F) of various sizes and shapes enclosed in chromitite. Note that the total thickness of the chromitite above and below the anorthosite blocks (except B) is commonly less than that of chromitite layers elsewhere. Note also that layer contacts are deflected around the anorthosite blocks. GPS coordinates: (A) point 351, latitude −24.910825° and longitude 30.103321°; (B) point 365, latitude −24.91056° and longitude 30.103416°; (C) point 349, latitude −24.910886° and longitude 30.103341°; (D) point 331, latitude −24.910788° and longitude 30.103483°; (E) and (F) point 340, latitude −24.911485° and longitude 30.103158°.

that the chromitite layers in some instances must have solidified sufficiently to behave in a brittle manner, while the surrounding anorthosite still retained sufficient melt to be mobile.

4.4. Thin offshoots of chromitite into anorthosite

Some thick, laterally continuous chromitite layers show offshoots of chromitite, ranging from 1 mm to several centimetres in thickness (Fig. 17). These offshoots bifurcate both downwards (Fig. 17B, D) and upwards (Fig. 17C, E) at high angles and pinch out within anorthosite at a distance of a few cm to dm. One much thicker and longer offshoot splits off the main UG1 layer into the underlying anorthosite (Fig. 18). It becomes thicker deeper into the anorthosite and then ends abruptly. These offshoots are different from the chromitite protrusions described above (Figs. 10 and 11). The protrusions show highly intricate contacts with adjacent anorthosite (Fig. 10E) and locally-derived anorthosite inclusions (Fig. 11). These are not features of the chromitite offshoots (Figs. 17 and 18).

5. Petrography of anorthosite and chromitite

5.1. Orthopyroxene oikocrysts in anorthosite

Ortho- and rarely clinopyroxene oikocrysts with the apparently dendritic outlines are commonly within the anorthosite layers associated with the UG1 chromitites (Fig. 3B). They are generally several decimetres wide and appear to have grown within a plagioclase mush, locally downwards (Fig. 19A) or sideways (Fig. 19B). Some pyroxene oikocrysts occur in association with zones in which

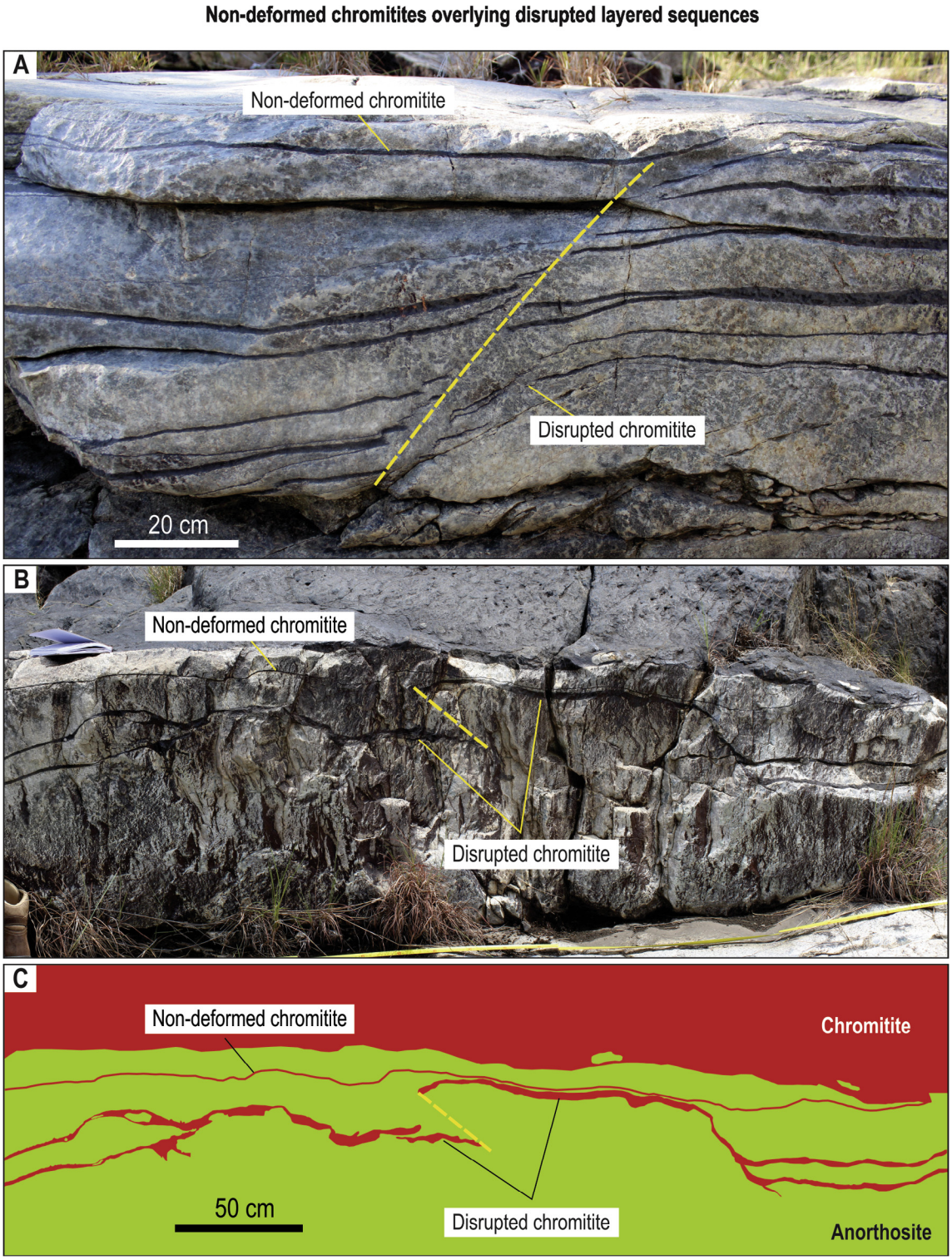

Fig. 9. Photographs and a corresponding sketch of disrupted chromitite layers overlain by nearly planar and non-deformed layers. (A) Disrupted bifurcating chromitite layers overlain by a planar and non-deformed chromitite layer. The yellow line demarcates a downward displacement of layers along a sealed normal fault. (B) A disrupted chromitite seam overlain by a nearly planar and non-deformed chromitite seam. (C) A sketch of (B) highlighting a thin almost planar chromitite seam that overlies a deformed and displaced chromitite layers. The yellow line demarcates an upward displacement of a chromitite layer along a sealed reverse fault. GPS coordinates: (A) point 342, latitude −24.911036° and longitude 30.103193°; (B) and (C) point 353, latitude −24.910856° and longitude 30.103205°. (For interpretation of the references to colour in this figure legend, the reader is referred to the web version of this article.)

chromitite layers were deformed in a brittle and ductile manner. Importantly, these pyroxene oikocrysts have overgrown the zones of deformation (Fig. 19C–F) and show no evidence of deformation. This indicates that the oikocrysts crystallized after both the formation of the chromitite layers and their deformation. The chromitite layers do not cut through the oikocrysts, as envisaged by some

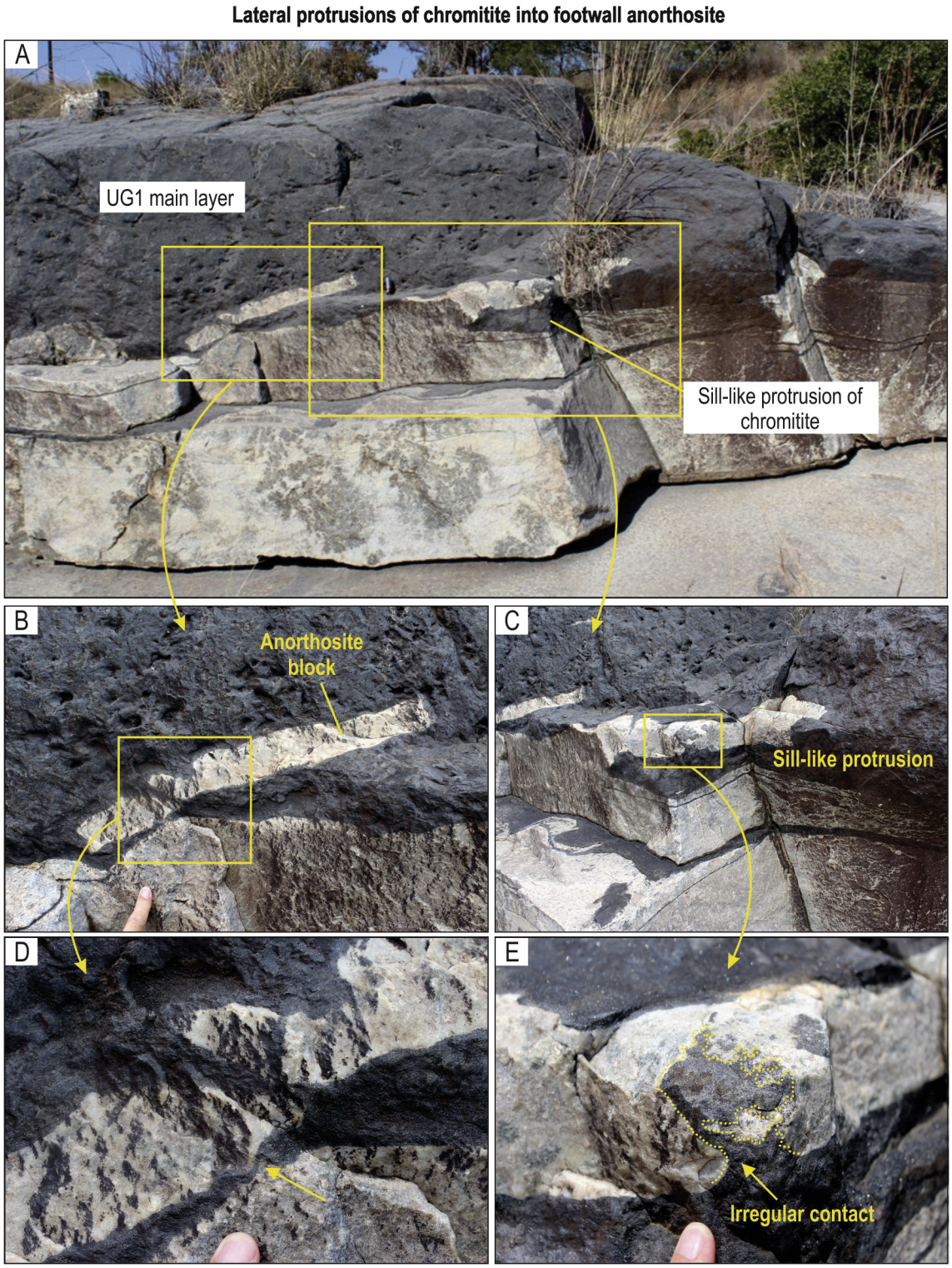

Fig. 10. Photographs of a sill-like protrusion of chromitite in footwall anorthosite and associated features. (A) An outcrop showing a chromitite that protrudes from the UG1 chromitite into the footwall anorthosite. (C) and (E) Close-ups illustrating the intricate shape of the contact (indicated by an arrow) between the protrusion and the overlying anorthosite. (B) and (D) An anorthosite block with a lower contact that roughly matches the upper contact of the underlying anorthosite (indicated by arrow). GPS coordinates: point 356, latitude −24.910852° and longitude 30.103191°.

researchers (e.g. Voordouw et al., 2009; Maier, pers. com., 2016). This inference is confirmed by our petrographic observations that orthopyroxene oikocrysts occur as optically continuous interstitial phases across both chromitite layers and adjacent anorthosite. The same relationships have been noted earlier by Wager and Brown (1967, p. 365) who stressed that large poikilitic orthopyroxenes pass into adjacent chromitite layers and are in optical continuity across the boundaries between chromitite and anorthosite layers. Mottled anorthosite invariably contains about 1 vol.% of chromite and should therefore be regarded as plagioclase-chromite cumulates.

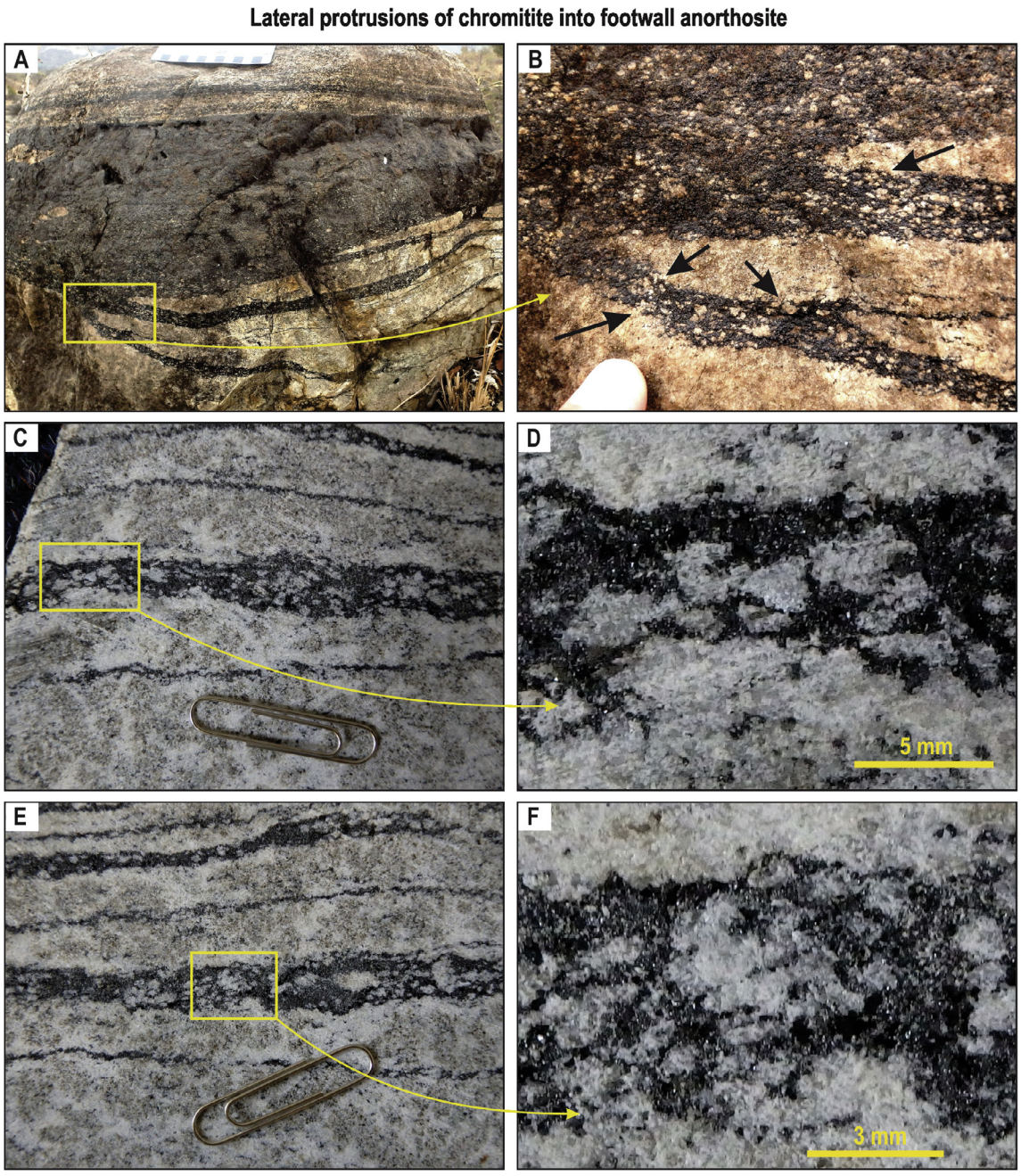

Fig. 11. Photographs of a thick chromitite layer that is continuous with thinner protrusions into the footwall anorthosite (A) and close-up of the same outcrop (B) showing the fritted contacts with anorthosite and the numerous small anorthosite inclusions, some of which are attached to footwall and hanging wall anorthosite (indicated by arrows). Photographs of the slab's surfaces (C, E) and corresponding close-ups (D, F) from the same outcrop illustrating anorthosite inclusions in narrow chromitite protrusions that appear to be connected both to each other and adjacent anorthosites. Most of these inclusions are probably autoliths produced by the *in situ* disintegration of the host anorthosite (see also Fig. 5). GPS coordinates: point 375, latitude −24.909606° and longitude 30.104083°.

5.2. Plagioclase oikocrysts in chromitite

Interstitial plagioclase occurs within most chromitite layers as idiomorphic, rectangular oikocrysts (the light patches in Figs. 12 and 20A–B). Their spatial distribution within the layers appears to be random. Interstitial orthopyroxene occupies spaces between plagioclase oikocrysts and form oikocrysts of irregular shapes (dark areas in Figs. 12 and 20A–B). A close inspection shows, however, that in many places there is more interstitial plagioclase in chromitite layers along their contacts with the host anorthosite and locally poikilitic plagioclase forms almost continuous rims (Fig. 20C–D). In chromitites, chromite forms discrete grains or clusters that are locally arranged in sub-vertical chains. These are poikilitically enclosed by plagioclase and orthopyroxene. The grains that are about 0.02 mm in size tend to be ovoid in shape whereas the relatively larger (up to 0.8 mm wide) grains exhibit subhedral shapes. Chromite in chromitite layers forms 40 to 60 vol.% apparently indicating their original enrichment in interstitial melt. In rare almost monomineralic layers, chromite may reach 90–95 vol.%. Despite the generally low abundance of chromite in chromitite layers, textures suggest that they are chromite cumulates.

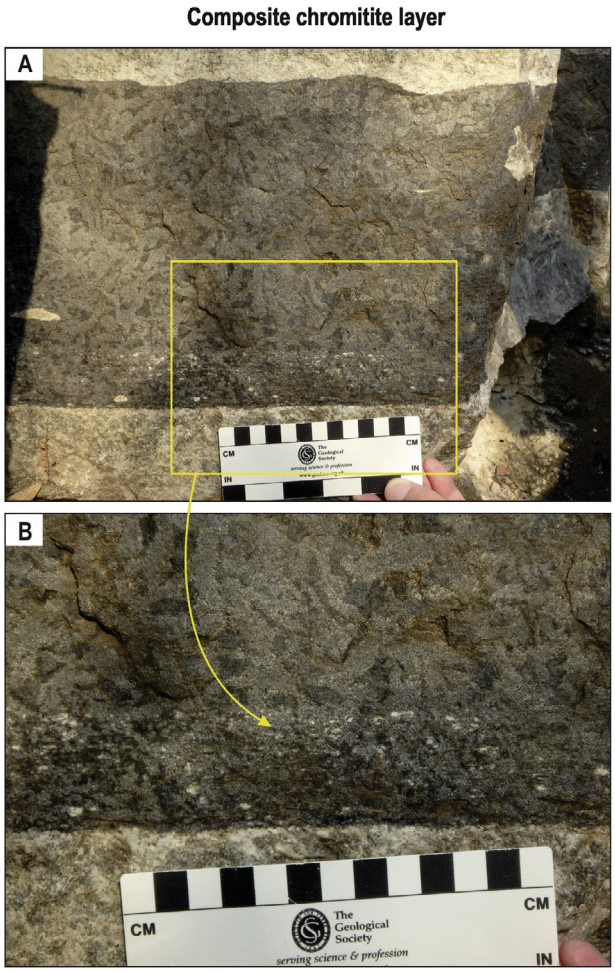

Fig. 12. Photographs of a composite chromitite layer (A) composed of the thicker uppermost sublayer of a massive coarse-grained chromitite with some large anorthosite autoliths and the thinner lowermost one of a finer-grained chromitite with numerous small anorthosite inclusions. A close-up (B) shows the thin basal sublayer. Note that, in contrast to Fig. 5, there is no evidence of *in situ* disintegration of the footwall anorthosite. GPS coordinates: point 334, latitude −24.911658° and longitude 30.103252°.

6. Hypotheses for bifurcating chromitite layers

The anorthosite-chromitite interlayering with bifurcating chromitites (Fig. 3) is a great challenge for existing hypotheses for the origin of igneous layering in mafic-ultramafic layered intrusions. Field observations show that the principal reason for the convergence and divergence of chromitite layers and the way that they bridge different stratigraphic levels is the occurrence of lenses of anorthosite isolated within the chromite cumulates. It is therefore not surprising that all hypotheses address, in one way or another, the origin of the lenses. Three major groups of models can be envisaged to explain the origin of this enigmatic layering: (1) The local *deposition* of lenses of anorthosite on the chamber floor, repeatedly followed by the crystallization of continuous chromitite (e.g. Ferguson and Botha, 1963; Cawthorn, 2003, 2015; Nex, 2004); (2) *Intrusion* of chromite-rich mush or chromite-saturated melt along anastomosing fractures in anorthosite (e.g. Cameron, 1963, 1964, 1978; Lee, 1981; Maier and Barnes, 2008; Voordouw et al., 2009; Maier et al., 2013; Mukherjee et al., 2017); (3) Plastic *deformation* of interlayered anorthosite and chromitite resulting in local merging of chromitite layers where anorthosite lenses pinch out (this study).

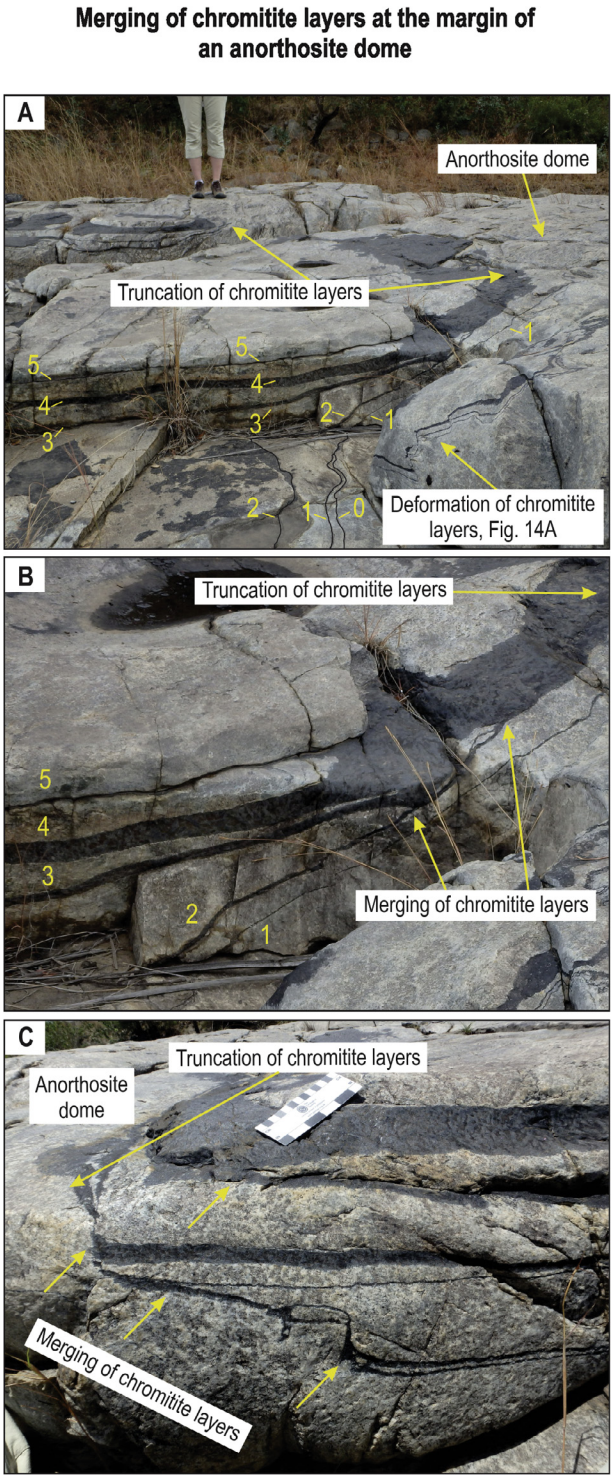

Fig. 13. Photographs illustrating the merging, truncation and deformation of chromitite layers at the margin of an anorthosite dome (A-C). See text for further discussion. GPS coordinates: point 371, latitude −24.910421° and longitude 30.103567°.

6.1. A depositional model

Igneous layering is traditionally thought to form by various processes involving accumulation of crystals on the floor of a chamber by sedimentary-type processes and/or *in situ* crystallization. Three major scenarios have been suggested to explain chromitite bifurcation in the context of this classical concept.

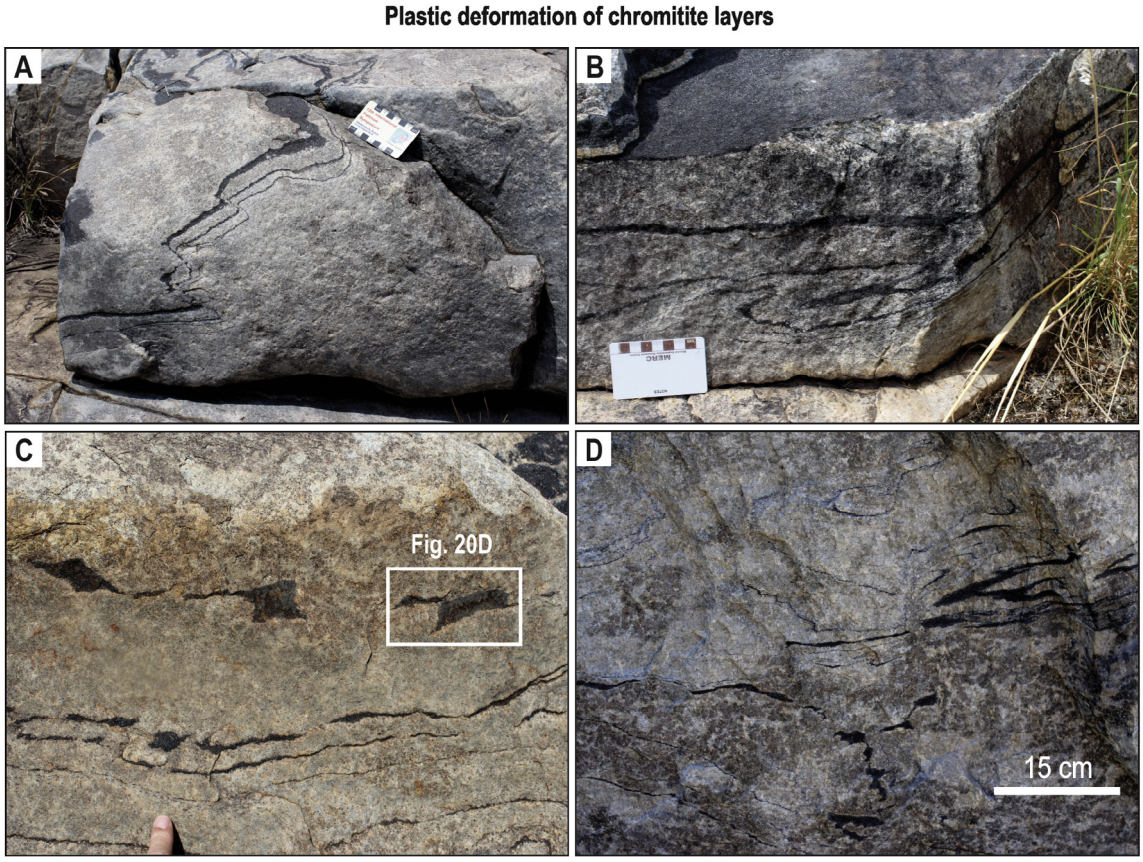

Fig. 14. Photographs of plastically deformed chromitite layers within mottled anorthosite. (A) Plastically deformed chromitite layers, which have retained continuity of the layering. (B) Plastically folded chromitite layers overlain by a planar and non-deformed chromitite layer. (C) and (D) plastically deformed and partly dismembered chromitite layers, which have lost some of their continuity. GPS coordinates: (A) point 371, latitude −24.910421° and longitude 30.103567°; (B) point 372, latitude −24.910172° and longitude 30.103721°; (C) point 373, latitude −24.910125° and longitude 30.103748°; (D) point 370, latitude −24.910447° and longitude 30.103523°.

The first detailed scenario was proposed by Cawthorn (2003). His model assumes the initial formation of a continuous layer of chromitite crystals on the chamber floor by settling of chromite from the overlying magma (Fig. 21A–B). This was followed by the patchy *in situ* crystallization of plagioclase resulting in isolated anorthosite lenses on the continuous layer of chromitite (Fig. 21 C). Subsequently, the crystallization of plagioclase was terminated by renewed settling of chromite to form another continuous chromitite that blankets the anorthosite lenses (Fig. 21 D). This sequence of events results in two chromitite layers diverging and converging around anorthosite lenses (Fig. 21 D). Multiple repetitions of this sequence of events could lead to a complex sequence of numerous anorthosite lenses separated by bifurcating layers of chromitite. The major weakness of this model is that it involves assumptions that may not be realistic. In particular, it does not clarify how the parent magma becomes saturated alternatively in chromite and plagioclase and what causes the switching between these two conditions. The model also appears to neglect the possible replenishment of the magma chamber. This is problematic as it does not satisfy mass balance requirements. Typical basaltic magmas will only contain a limited amount of Cr (~1000 ppm) and therefore any event that results in saturation of the resident magma in chromite will only be able to produce a single layer of massive chromitite. Any subsequent events will not result in chromitite because the resident magma has already been depleted in Cr. Thus, without additions of Cr-undepleted magma there cannot be multiple chromitites. More importantly, the model does not explain the field relations such as lobate and highly irregular contacts between layers (Figs. 4 and 5), disintegration of footwall anorthosite (Figs. 5, 11 and 12), planar chromite layers above disrupted portions of the cumulate pile (Fig. 9) and sill-like protrusions of chromitite into footwall anorthosite (Figs. 10 and 11).

A later attempt to explain the chromitite bifurcation was presented by Nex (2004) who emphasised the existence of metre-scale domal structures in which anorthosite disrupt the originally continuous chromitite layers. The model attributes chromitite bifurcations to the simultaneous operation of two independent processes: (a) settling of chromite to form continuous chromitite layers on the chamber floor (Fig. 22A) and (b) the emplacement of plagioclase-rich mush derived from underlying anorthositic cumulates (Fig. 22B–C). Saturation of the magma in chromite is attributed to periodic replenishment of the chamber by new pulses of crustally-contaminated magma. Seismic activity associated with these influxes is suggested as a trigger for the liquefaction of the uppermost part of the cumulates (to a depth of ~10 m) and its repeated extrusion as plagioclase-rich mush much like a sand volcano on the chamber floor forming the localised anorthosite lenses (Fig. 22C). The settling chromite forms another chromitite layer that converges with the previous one between anorthosite lenses, thus forming the chromitite bifurcations (Fig. 22D). The advantage of this hypothesis is that it does not require repeated switching from chromite- to plagioclase-saturated magmas, although the origin of the footwall anorthosite remains unexplained. It also overcomes the mass balance problem because multiple replenishment events could continuously bring Cr-undepleted magmas into the chamber. The major problem is that the model

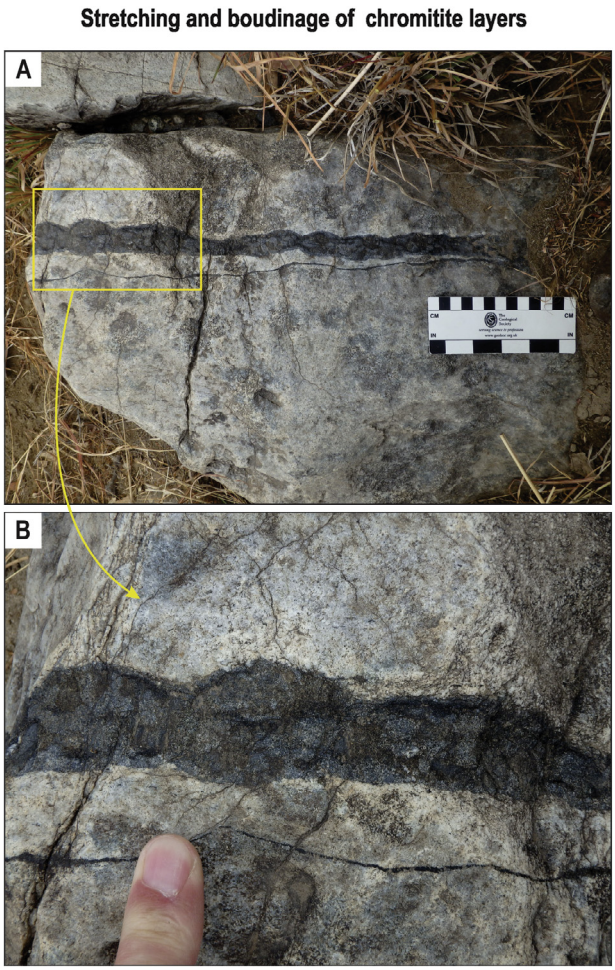

Fig. 15. Photographs of a chromitite layer that was stretched and boudinaged within mottled anorthosite. GPS coordinates: point 337, latitude −24.911642° and longitude 30.103097°.

does not account for the complex contacts between chromitite and anorthosite layers (Figs. 4, 5 and 11). However, as detailed below, anorthosite domes do appear to result in some chromitite bifurcation but not in the way envisaged in this model.

Another variant has been recently put forward by Cawthorn (2015 and 2016, pers. comm.) in which he suggested a sedimentological analogy in a closed system as the simplest interpretation for chromitite bifurcation. It is envisaged that initially the magma in the chamber was saturated in three minerals – orthopyroxene, chromite and plagioclase. The first two minerals settled to the chamber floor forming chromite-bearing orthopyroxenite, leaving a suspension of plagioclase crystals in the magma (Fig. 23A). The plagioclase crystals settled from downward moving convection currents forming elongated anorthosite lenses on the chamber floor (Fig. 23A, C); elsewhere plagioclase was still held in suspension. The process was complicated by earthquake-related shock waves that initiated nucleation of chromite grains (the mineral with the simplest structure) everywhere in the chamber, which settled through the plagioclase suspension onto the chamber floor, producing thin but continuous chromitite layers (Fig. 23B, D). Repeated earthquakes caused the formation of large number of thin chromitite layers, while the plagioclase continued to accumulate as discontinuous layers between each chromitite layer. Thus, chromitite bifurcation resulted from the two distinct mechanisms of deposition: discontinuous anorthosite lenses separated from descending suspensions and continuous chromitite layers from earthquake-triggered nucleation throughout the entire chamber (Fig. 23).

This model faces the following problems: (1) It requires perfect separation of all orthopyroxene crystals from all plagioclase crystals so that only the latter remained suspended in the magma (Fig. 23A). This follows from the observation that orthopyroxenite and overlying anorthosite interlayered with chromitite do not appear to contain any cumulus plagioclase and orthopyroxene, respectively. It is difficult to imagine that gravity settling could result in such a perfect separation of these two minerals; (2) The physical separation of chromite from suspended plagioclase presents an even bigger problem. The fact that chromite is much denser than plagioclase does not mean that it will be the first to settle from a magma. It is the size of crystals that principally governs their settling velocity and co-crystallizing silicate minerals are commonly one to two orders of magnitude larger than chromite (e.g. Roeder et al., 2006). Since the radius of crystals is raised to the power of two in the Stokes' equation, the plagioclase would sink 10–20 times faster than chromite crystals (e.g. Hess, 1960). This leaves little possibility for chromite to settle and form layers of monomineralic chromitite on the chamber floor; (3) The absence of cumulus orthopyroxene in anorthosite and chromitite layers implies that after the initial separation of all orthopyroxene crystals on the chamber floor, the magma was unable to crystallize orthopyroxene again. It is not clear why multiple seismic events failed to bring it back onto liquidus despite the magma being nominally saturated in orthopyroxene (along with chromite and plagioclase); (4) Seismic waves will not prevent convective currents and therefore deposition of plagioclase on the chamber floor must take place on a more-or-less continuously together with chromite. If so, it is not clear why the chromitites are essentially devoid of cumulus plagioclase. There appears to be no process that would prevent deposition of plagioclase on the chamber floor during periods of chromite accumulation; (5) Closed-system conditions are not compatible with generation of multiple layers of chromitite (with a total thickness of about 1.5–2 m) from Cr-poor basaltic magmas. This mass balance issue can only be resolved by replenishment of the chamber by new pulses of Cr-undepleted magma; (6) No explanation is provided for all of the complex field relations between anorthosites and chromitites (Figs. 4–12).

6.2. An intrusive model

Sampson (1932) pioneered an intrusive model by suggesting that a residual melt near chromite in composition intruded underlying, solidified and fractured anorthosite. The idea was subsequently abandoned when it became clear that melts of such composition do not exist in nature. Three modified versions of the intrusive hypothesis have since been proposed. The first, by Cameron (1963, 1964, 1978) and Lee (1981), invoked chromite-rich mush dilating fractures in anorthosite. The driving force for the post-depositional deformation of cumulate pile was supposed to be the density difference between chromitite and anorthosite. Lee (1981) proposed that heavy chromite-rich mush overlying anorthosite (Fig. 24A–B) may collapse along pre-existing fractures into underlying anorthosite (Fig. 24C) and solidified into laterally continuous and bifurcating chromitite sills (Fig. 24D). One could also speculate that chromite-rich mush may have been sucked or squeezed upwards into opening fractures within overlying anorthosite (Fig. 24C–D). The hypothesis is appealing in its simplicity and is consistent with some field relations. In particular, thin offshoots from thicker chromitite layers extending into surrounding anorthosite (Figs. 17 and 18) could be indeed attributed to post-depositional mobilisation and intrusion of chromite-rich mush into footwall and hanging wall rocks. The process appears to result, however, in the formation of a distinct and localised

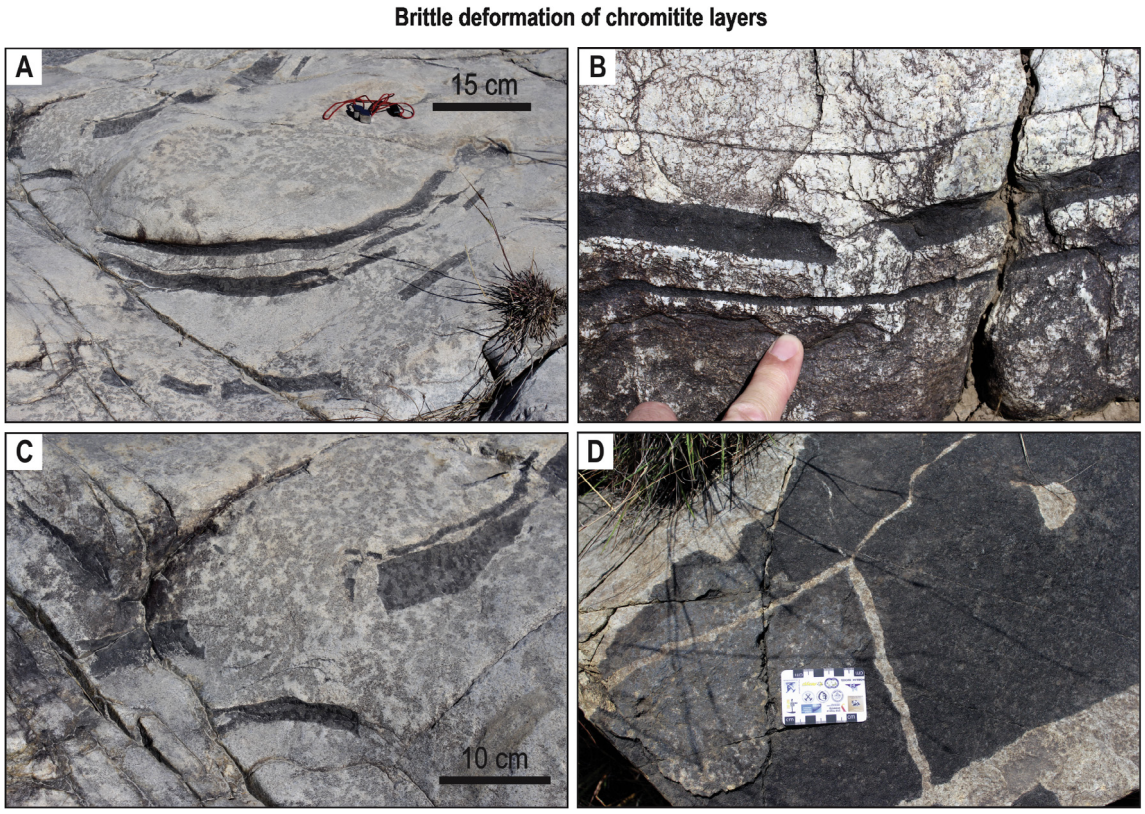

Fig. 16. Photographs of chromitite layers affected by brittle deformation within mobilised plagioclase cumulate. (A) Disrupted chromitite layers. (B) Cross-section of a disrupted chromitite layer sandwiched between two thinner non-deformed chromitite layers. (C) Displaced blocks of disrupted chromitite layers (detail of A). (D) Plan view of dismembered chromitite layer with anorthosite filling in the gaps between the fragments. GPS coordinates: (A), (B) and (C) point 338, latitude −24.911523° and longitude 30.103044°; (D) point 339, latitude −24.911434° and longitude 30.103083°.

variety of chromitite bifurcation with no anorthosite lenses between chromitite layers (Figs. 17 and 18). This post-depositional variety is easily recognizable in the field and does not correlate with the prevailing type of chromitite bifurcation (Fig. 3).

A second version of the intrusive concept suggests that UG1 chromitite layers did not form directly on the chamber floor but rather within the cumulates from chromite-rich slurries that either segregating from slumping cumulates (Maier and Barnes, 2008; Maier et al., 2013) or arriving from a deeper-seated magma chamber (Voordouw et al., 2009). We will only examine here the scenario by Voordouw et al. (2009) because it was specifically developed for the bifurcation of UG1 chromitite layers. Their idea is depicted in Fig. 25, where chromite-rich slurries (with ~50–60 vol% chromite) were injected into pre-existing fractures within anorthosite. It is envisaged that some of the fracture zones undulate (Fig. 25A, B) such that the continued injection of the slurries resulted in chromitite bifurcation (Fig. 25C, D). This hypothesis appears to be simple and straightforward but has several serious problems. First, given the high density of the chromite it is hard to envisage that chromite-rich slurries could be transported from a deeper chamber and intruded into the Bushveld chamber. Second, the hypothesis requires fractures to extend several kilometres. It is difficult to imagine that chromite-rich slurries could successfully propagate through narrow fractures for such a long distance. In addition, horizontal fracture zones have not been documented in layered intrusions. Third, the late intrusion of chromitites requires brittle deformation and fracturing of anorthositic cumulates. There is, however, no evidence for this (Nex, 2004). Fourth, orthopyroxene oikocrysts are not crosscut by the UG1 chromitite seams as cited by Voordouw et al. (2009). Field and textural observations indicate that the oikocrysts grow from interstitial liquid after the formation and deformation of the chromitite-anorthosite layering (Fig. 19). Fifth, field relationships suggest that chromitite layers form directly on the chamber floor, not within the cumulate pile, disproving the intrusive origin of chromitites (see below). As mentioned above, thin offshoots of chromitite do exist in anorthosite (Figs. 17 and 18) but can be easily explained in the framework of the previous model (Fig. 24). Their existence does not require such a radical mechanism for origin of chromitites as implied by the Voordouw et al. (2009) model. Sixth, if the UG1 chromitites are separate sills, then they must have crosscutting relationships with their surrounding solidified cumulates, in particular, with the hanging wall rocks. In reality, the reverse is the case. We have recently documented potholes in the Impala Platinum Mine that cut down through the UG1 chromitites and are filled by overlying cumulates. This clearly indicates the UG1 chromitites form in sequence with the associated cumulate rocks and not as sills intruded into pre-existing cumulates.

Finally, a third version of the intrusive model has been proposed recently by Mukherjee et al. (2017) to explain an impressive apophysis of the UG1 chromitite that extends into footwall anorthosite from a pothole entirely composed of chromitite. They proposed that the chamber was replenished by dense, superheated melt that caused thermochemical erosion of the pre-existing floor cumulates and subsequently crystallized chromitite on the chamber floor. The chromitite protrusion is attributed to *in situ* crystallization of the chromite-saturated melt in a sill-like cavity produced by thermochemical erosion of cumulate rocks. The idea that some of chromitite layers may indeed represent intrusions

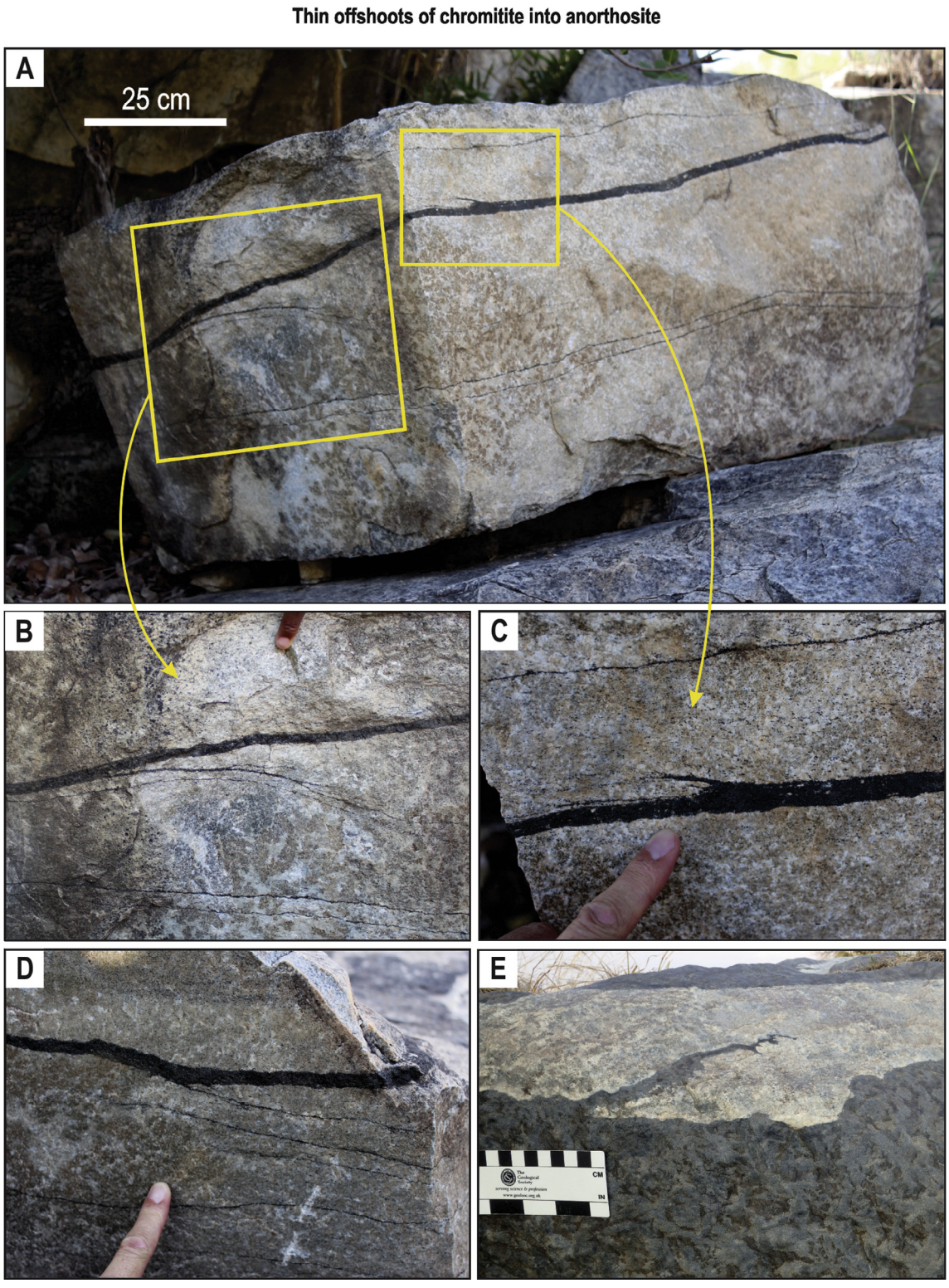

Fig. 17. Photographs of thin offshoots of chromitite within mottled anorthosite. (A) Photograph of a boulder showing several chromitite layers of different thickness. The thickest layer exhibits chromitite offshoots in both the overlying and underlying anorthosite. (B) and (D) Less than 1 mm thick chromitite offshoots branching from a thicker chromitite layer downwards into the footwall anorthosite. (C) and (E) about 3 to 10 mm thick chromitite offshoots that branch from the thicker chromitite layer upwards into the hanging wall anorthosite. Note that all offshoots characteristically branch off at high angles and terminate abruptly over distances of only a few cm to dm. GPS coordinates: (A), (B) and (C) and (D) point 346, latitude −24.910967° and longitude 30.103286°; (E) point 360, latitude −24.910664° and longitude 30.103400°.

in the footwall is strongly supported by our field observations on inclusion-rich chromitite seams (Fig. 11). We interpret these seams as injections into footwall anorthosite because they contain anorthosite inclusions that are partly attached to the footwall and hanging wall. The fact that the seams are locally almost choked with *in situ* inclusions is difficult to reconcile with forceful

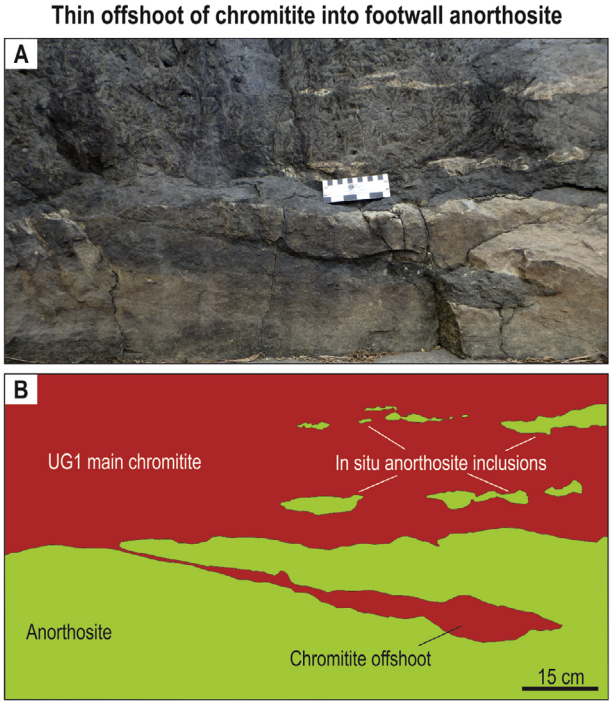

Fig. 18. Photograph (A) and sketch (B) of a thin offshoot of chromitite extending from the main UG1 layer into footwall mottled anorthosite. Note that the offshoot branches off at high angle and abruptly terminates after a short distance. GPS coordinates: point 368, latitude −24.910408° and longitude 30.103452°.

emplacement of chromite-rich mush which would physically displace any inclusions from the channels. Rather, this is compatible with the percolation of chromite-saturated liquid along fractures, resulting in thermal/chemical erosion of anorthosite (Fig. 26A–B) followed by *in situ* chromite crystallization from continuously flowing liquid (Fig. 26C–D). The important feature in this case (Fig. 11) is that the process of erosion and crystallization is essentially caught in action. It should be noted, however, that this specific type of chromitite bifurcation is not the principal one that we address in this study (Fig. 3).

6.3. A deformational model

Some of the complex field relationships between chromitites and anorthosite can be interpreted as resulting from 'soft-sediment deformation' associated with mobile anorthosite. In this context chromitite bifurcations can be attributed to post-cumulus ductile deformation of cumulates in response to diapir-induced stresses (Fig. 27A, B). It is envisaged that the redistribution of mobile anorthosite mush (Fig. 27C) may result in local convergence of chromitite layers that were initially separated (Fig. 27D). The possibility is supported by the observation of merging chromitite layers around anorthosite domes (Fig. 13). Superficially, this results in chromitite bifurcation (and even anorthosite lenses) but it is post-depositional and, has little to do with the type of chromitite bifurcation (Fig. 3) which is the subject of the present study. The primary chromitite bifurcation is localised (e.g. Fig. 3B, C) and does not have any obvious connection with anorthosite diapirs. The stresses required to form bifurcations over small, often only cm-wide, distances are hard to envisage. For this reason, we believe that deformation is unlikely to be the sole agent for chromitite bifurcation. Rather, deformation has only modified pre-existing chromitite bifurcation by ductile and brittle deformation of the cumulates (Figs. 13–18).

7. A novel hypothesis for chromitite bifurcations

7.1. The implications of field relations for magma chamber processes

In a series of recent publications (Latypov et al., 2015, 2017; Mukherjee et al., 2017) it has been asserted, in accord with many previous studies (e.g. Vermaak, 1976; Kruger and Marsh, 1985; Campbell, 1986; Eales et al., 1988; Maier and Eales, 1997; Smith et al., 2003; Cawthorn et al., 2005; Roberts et al., 2007; Naldrett et al., 2011), that magmatic (i.e. thermal and chemical) erosion of footwall cumulates is a very common feature in the BIC. We attribute the erosion to replenishment of the chamber by new magmas that were superheated, due to either magma mixing or adiabatic ascent (Latypov et al., 2015, 2017). On a large scale, depressions in the chamber floor (so-called potholes) below the Merensky Reef and UG2 chromitite layers, in which parts of the footwall succession are missing, are widely considered as robust evidence for magmatic erosion of the footwall (e.g. Vermaak, 1976; Kruger and Marsh, 1985; Campbell, 1986; Viring and Cowell, 1999; Cawthorn et al., 2005; Naldrett et al., 2011). On a smaller scale, uneven contacts below the Merensky Reef (e.g. Eales et al., 1988; Smith et al., 2003; Latypov et al., 2015, 2017) have been attributed to erosion. We note that sharp, planar contacts do not necessarily exclude magmatic erosion but can simply reflect uniform erosion resulting in no obvious discordance between different lithologies (e.g. Latypov et al., 2015). The present study provides additional evidence for the importance of magmatic erosion in the evolution of the BIC.

7.1.1. Insights from irregular contacts, disintegration of footwall anorthosite, termination of anorthosite layers and wispy anorthosite inclusions

We interpret the wavy contacts between anorthosite and UG1 chromitite (Fig. 4) as a consequence of magmatic erosion of the cumulate pile during the formation of this sequence of layers. Note that the uneven contacts cannot arise from the late stage ductile deformation since there are planar upper contacts to anorthosite layers (Fig. 6A, C). The lobate contacts between chromitite and overlying anorthosite must be a primary magmatic feature that was developed directly at the chamber floor. Importantly, the wavy surfaces are characteristic of the upper contacts of both chromitite (Fig. 4A–C) and anorthosite (Fig. 4D) layers. This suggests that magmatic erosion may have immediately predated formation of both chromitite and anorthosite. The process of magmatic erosion seems to have been arrested in action in places where progressive disintegration of footwall anorthosite into numerous small inclusions, some of which are attached to each other and with footwall anorthosite, is evident (Fig. 5). We consider these examples of anorthosite disintegration as strong and direct evidence for magmatic erosion.

The disappearance of some cumulate layers along the strike of the Critical Zone of the BIC is generally attributed to large-scale magmatic erosion (e.g. Eales et al., 1988). The same feature, but on a much smaller scale, is observed at the DRL where some anorthosite layers within massive chromitite disappear along strike over short distances (Fig. 6). We attribute the gaps and lateral terminations of anorthosite layers to magmatic erosion by new magmas that subsequently crystallized the overlying chromitite layers. In other words, the anorthosite lenses are remnants of previously continuous anorthosite layers that experienced irregular degrees of magmatic erosion. The wavy bases of some anorthosite layers (Figs. 4A–C and 6A, C) can be attributed to their deposition on the erosional surface of chromitites. Earlier, alternative interpretations for lateral terminations of anorthosite layers are sporadic accumulation or *in situ* growth of patches of

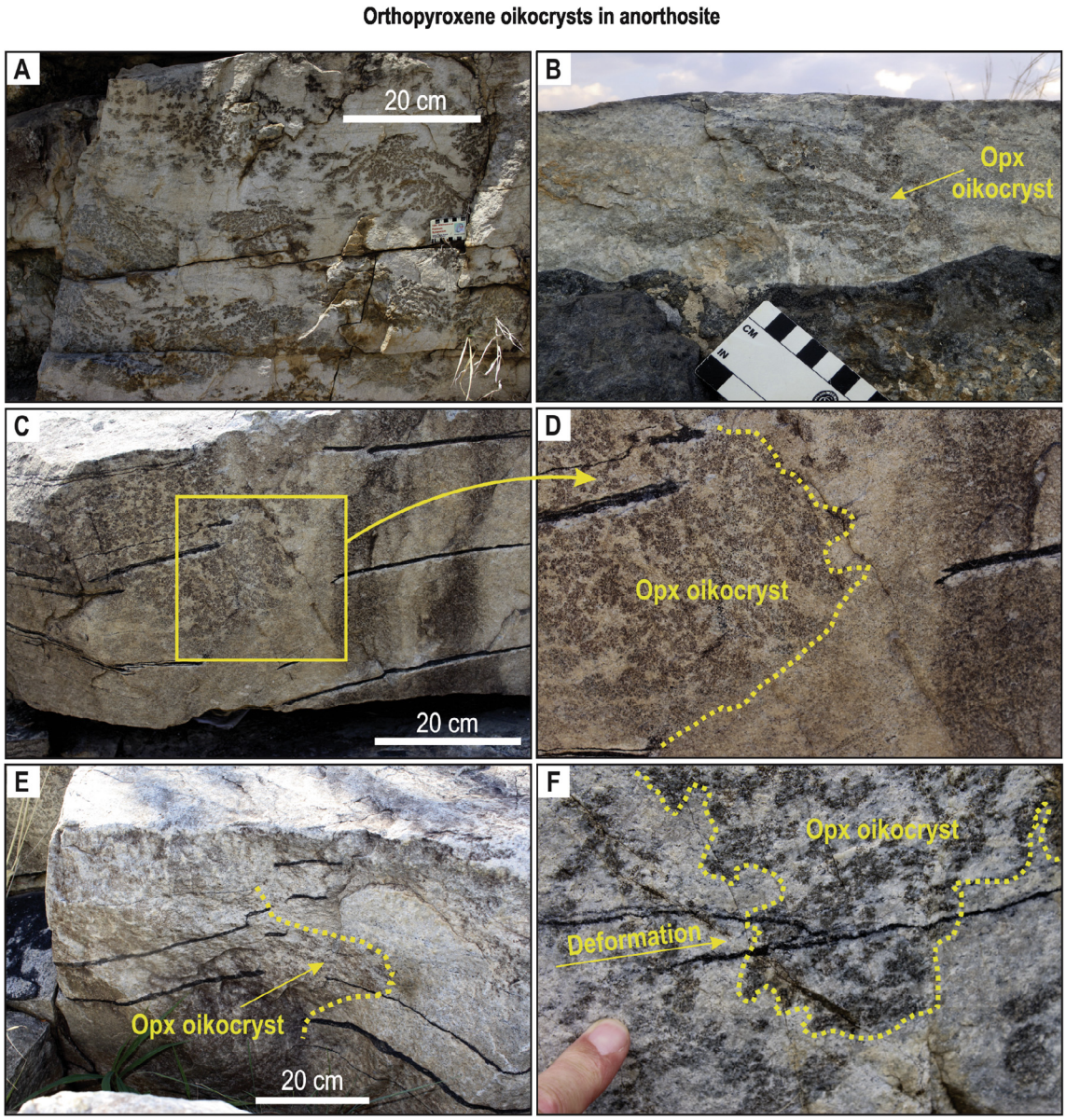

Fig. 19. Photographs of large oikocrysts of orthopyroxene within mottled anorthosite. (A) Orthopyroxene oikocrysts that branch downwards. (B) Orthopyroxene oikocrysts branching sideways. (C), (D) and (E) Orthopyroxene oikocrysts that overgrew zones of brittle and ductile deformation of chromitite layers. (F) Orthopyroxene oikocrysts postdating plastic deformation of a chromitite layer. GPS coordinates: (A) point 332, latitude −24.910615° and longitude 30.10361°; (B) point 367, latitude −24.91048° and longitude 30.103446°; (C) and (D) point 352, latitude −24.91141° and longitude 30.103134°; (E) point 345, latitude −24.910998° and longitude 30.103264°; (F) point 330, latitude −24.910846° and longitude 30.103493°.

anorthosite on the chamber floor (Cawthorn, 2003, 2015). These hypotheses could possibly explain to widely (several decimetre) spaced, thick anorthosite lenses but would require extremely localised deposition of plagioclase in a dynamic magma chamber, which is difficult to comprehend for millimetre-thick anorthosite lenses a few centimetres apart (Fig. 6B–C).

A further informative feature is the existence of anorthosite inclusions within chromitite layers (Fig. 7). These are commonly interpreted as fragments derived from the footwall sequence and transported in flowing magma. However, the delicacy of the wispy tails (Fig. 7B) to some of them argues against such an interpretation. As argued by Maier et al. (2013), it is unlikely that the tails could have survived transport of the inclusions through the magma chamber to the point of their final deposition. In addition, some anorthosite inclusions are penetrated by fingers of chromitite that passes into a thinner chromitite vein (Fig. 7D). The observation is difficult to reconcile with transport. Moreover, the highly uneven, almost scalloped, contacts of some anorthosite inclusions (Fig. 7C) together with the direct attachment of some of them to footwall anorthosite (Fig. 5B), suggest that they are *in situ* autoliths, i.e. non-transported remnants of previously continuous and largely eroded anorthosite layers.

Magmatic erosion of pre-existing cumulates requires that magmas parental to the chromitites (and anorthosites) were in contact with cumulates forming the temporary floor of the magma chamber. This could only be the case if any new hotter magma was relatively dense and spread out as a basal layer along the interface between the resident melt and the temporary chamber floor. This is an important deduction that must be incorporated into any successful hypothesis for origin of this layered sequence.

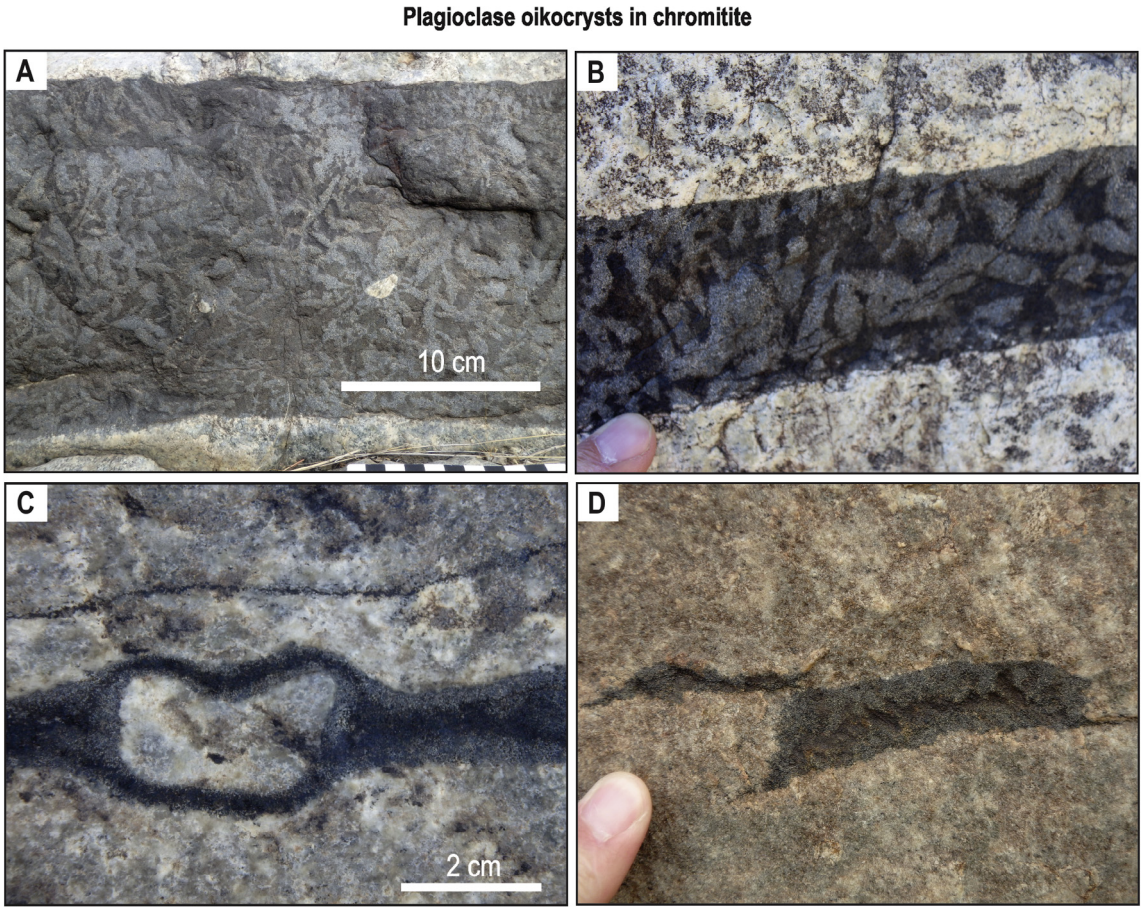

Fig. 20. Photographs documenting oikocrysts of plagioclase and pyroxene in UG1 chromitite. (A) and (B) Large lath-shaped plagioclase oikocrysts within chromitite layers. (C) Rims of interstitial plagioclase in chromitite surrounding an anorthosite inclusion and along contacts with both footwall and hanging wall anorthosite. (D) A rim of interstitial plagioclase developed along the periphery of part of a disrupted chromitite layer (see Fig. 14C). GPS coordinates: (A) point 359, latitude −24.910680° and longitude 30.103297°; (B) point 350, latitude −24.910881° and longitude 30.103336°; (C) point 355, latitude −24.910821° and longitude 30.103288°; (D) point 373, latitude −24.910125° and longitude 30.103748°.

7.1.2. Insights from disrupted and planar chromitite layers

Evidence of ductile and brittle deformation of chromitite layers is widespread at the DRL (Figs. 9, 13–16, 19C–F). It has been attributed to syn-magmatic localised upwelling of small anorthosite masses (Nex, 2004) or shock waves associated with tectonic or igneous events (Cawthorn, 2015). One intriguing aspect of this feature is that disrupted chromitite layers are commonly overlain by continuous, planar and non-deformed chromitite layers (Fig. 9). The planar chromitite layers thus appear to have no memory of the event that caused brittle disruption of underlying chromitite layers. This suggests that the planar layers post-dated the deformation and that it was deposited on a relatively flat and planar surface. Our preferred interpretation for these features is that chromitite layers (Fig. 28A) were disrupted by normal faults, resulting in a step-like surface (Fig. 28B). After deformation the topography of the cumulate pile was smoothed by syn-magmatic erosion of the chamber floor due to new magma replenishing the chamber (Fig. 28C). This was followed by deposition of a planar chromitite layer on the eroded, planar floor of the chamber (Fig. 28D). Several important implications can be drawn from this case: (a) the smoothing of the chamber floor topography is strong evidence for magmatic erosion of pre-existing cumulates; (b) the disruption of bifurcated chromitite layers indicates that bifurcation is the result of a syn-magmatic process that operates close to or directly on the chamber floor; (c) the existence of planar chromitite layers is evidence for deposition directly on the temporary floor of the magma chamber. Again, these processes imply that pulses of new magma were spreading as basal flows between the chamber floor and the overlying resident melt.

7.1.3. Insights from protrusions of chromitites

We consider the intricate contacts (Fig. 10E), inclined anorthosite inclusions (Fig. 10B) and matching contacts of the anorthosite block with the underlying anorthosite layer (Fig. 10D) as evidence for the emplacement of magmas parental to chromitites as basal flows capable of thermo-chemical erosion of pre-existing cumulates and detachment of some eroded blocks from the anorthosite footwall. The following events are envisaged (Fig. 29). First, magma penetrates weak zones (e.g. brittle fractures) within pre-existing plagioclase cumulates (Fig. 29A–B). This magma erodes upwards and downwards into the adjacent anorthosite. The forceful intrusion of the magma into anorthosite cumulate dislodged and rotated the anorthosite block away from the rest of the anorthosite layer. Chromite started to crystallize to eventually envelop the anorthosite block (Fig. 29C–D). For this process to take place, the inflowing magma must have been in contact with the anorthosite cumulates, it must have been very reactive in nature and it must have been capable of crystallizing chromite *in situ* beneath the anorthosite screen and on the chamber floor. The scenario is almost identical to the one presented above (Fig. 26); the only difference being that erosion of footwall rocks in this case was so effective that no evidence for progressive disintegration and

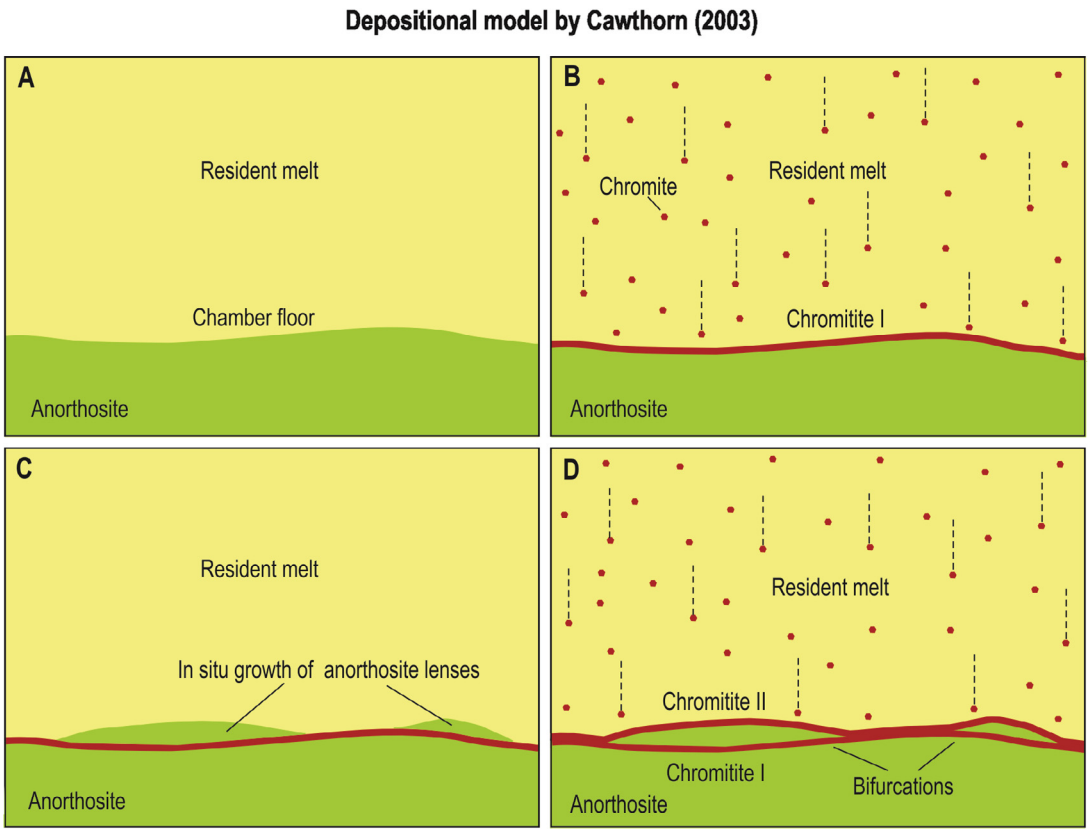

Fig. 21. A sketch of the depositional model proposed by Cawthorn (2003) for bifurcating chromitites. The central idea is that the anorthosite lenses responsible for the splitting of chromitite layers were the result of patchy *in situ* growth of plagioclase on the chamber floor. See text for the discussion.

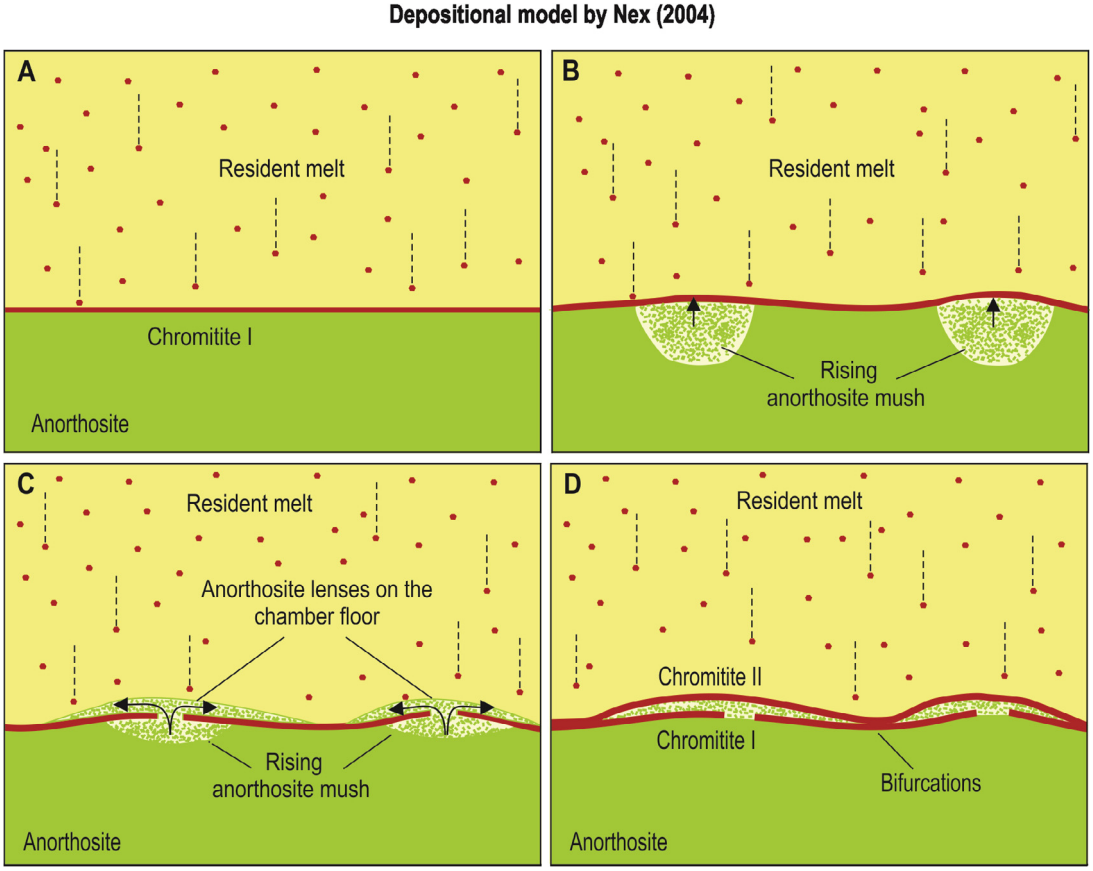

Fig. 22. An illustration of the depositional model of Nex (2004) for the formation of bifurcating chromitite. The principal claim is that the anorthosite lenses responsible for the divergence of chromitite layers were mobilised plagioclase cumulate that was erupted onto the chamber floor. See text for the discussion.

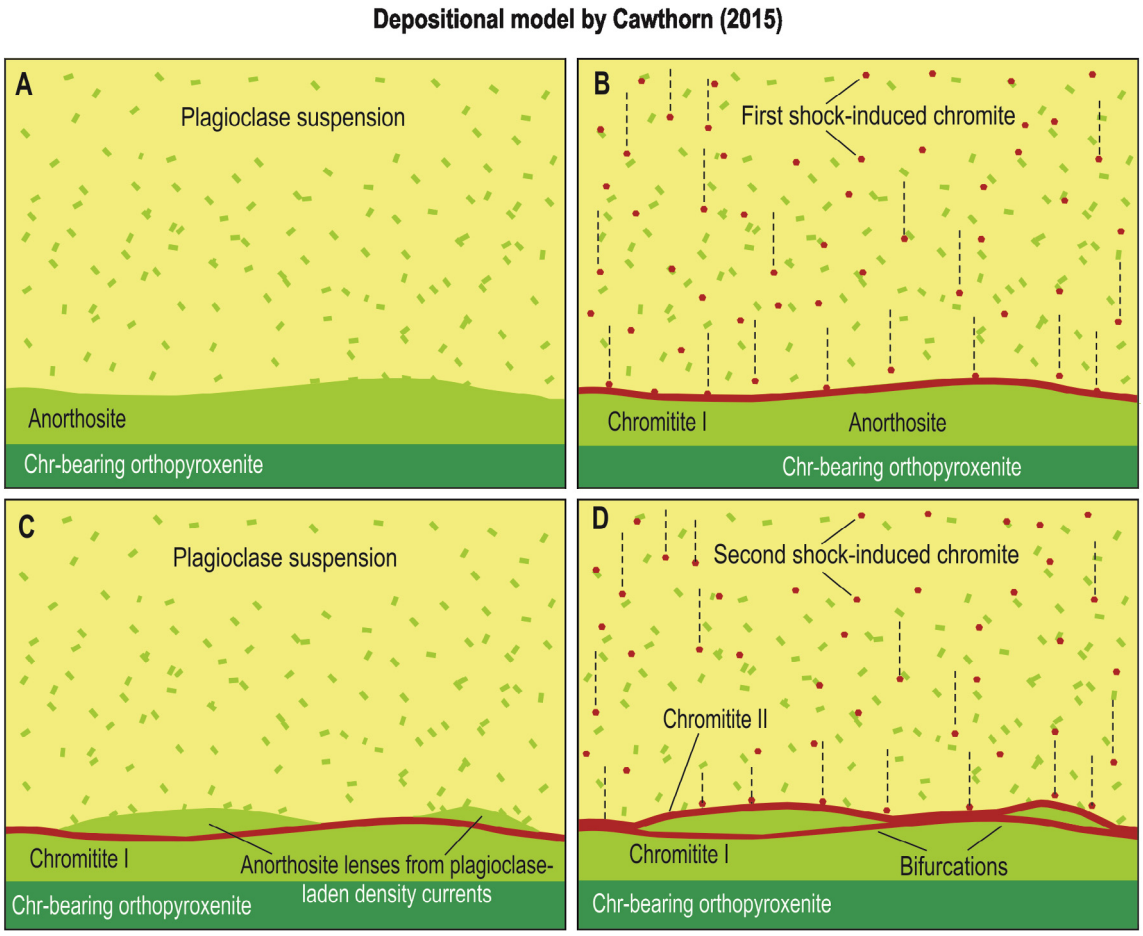

Fig. 23. A sketch of the depositional model advanced by Cawthorn (2015) for the formation of bifurcating chromitite. He suggests that the anorthosite lenses responsible for the divergence of chromitite layers were the result of localised deposition of suspended plagioclase crystals from the descending convecting currents. See text for the discussion.

digestion of anorthosite in the form of small inclusions are preserved in the rocks.

7.1.4. Insights from transported anorthosite blocks

Anorthosite blocks within chromitites (Fig. 8) are superficially like the anorthosite inclusions discussed above (and see Fig. 7) but are distinct in that adjacent layer contacts are deflected and the thickness of the enveloping chromitite decreases around them (Fig. 8). It is envisaged that these blocks are transported anorthosite autoliths, rather than *in situ* erosional remnants of pre-existing rocks. They were probably dislodged from pre-existing cumulates during replenishment events and settled into chromitite layers forming at the chamber floor like "drop-stones" in clastic sediments (Fig. 30A). Subsequent crystals of chromite then accumulated on top of the anorthosite blocks (Fig. 30B). Later compaction of the cumulates led to moulding of the chromitite layers around the blocks (Fig. 30C–D). The implication is that chromitite-anorthosite layering forms directly on the temporary floor of the magma chamber, not within the cumulate pile as implied in some hypotheses (e.g. Maier and Barnes, 2008; Voordouw et al., 2009; Maier et al., 2013).

7.2. Magma superheating and erosion of footwall cumulates

The field relations presented above indicate that erosion of pre-existing cumulates by newly emplaced magma was an inherent part of the process of chromitite formation. It seems most likely that cumulates were removed through melting and dissolution, with magma superheating appearing to be a necessary condition. If the replenishing magma had been saturated with some particular mineral, then it would have started to crystallize at once, covering and protecting the floor cumulates from erosion. If the magma contained phenocrysts, these could soon settle to the floor, also isolating it from dissolution. The field relationships thus require replenishing magmas to be unsaturated in all phases (i.e. to be superheated). Superheated magma is not normally a consequence of mantle melting or intra-chamber fractional crystallization (Latypov et al., 2015, 2017). One needs thus to have a physical mechanism that can result in magma superheat. One plausible mechanism is the rapid ascent of large volumes of magma from depth, so that cooling was negligible. This can result in superheating due to the difference in slope between the adiabatic gradient and the liquidus. This difference is about 3 °C/km so that the degree of superheating could be up to 10–30 °C for magma ascending from a storage region located at a depth corresponding to a pressure difference of about 10 kbar (an assumed position of a staging chamber at the Moho).

The erosion of footwall cumulates by superheated melt will take place during (1) lateral flow of magma across the floor during chamber replenishment and (2) vigorous convection in the basal layer after replenishment of the chamber. The rate of erosion at the first stage is relatively fast and may occur over several days to weeks. Basal flows are supposed to have formed as a high volume, rapidly emplaced surge over a chamber floor, leading to a

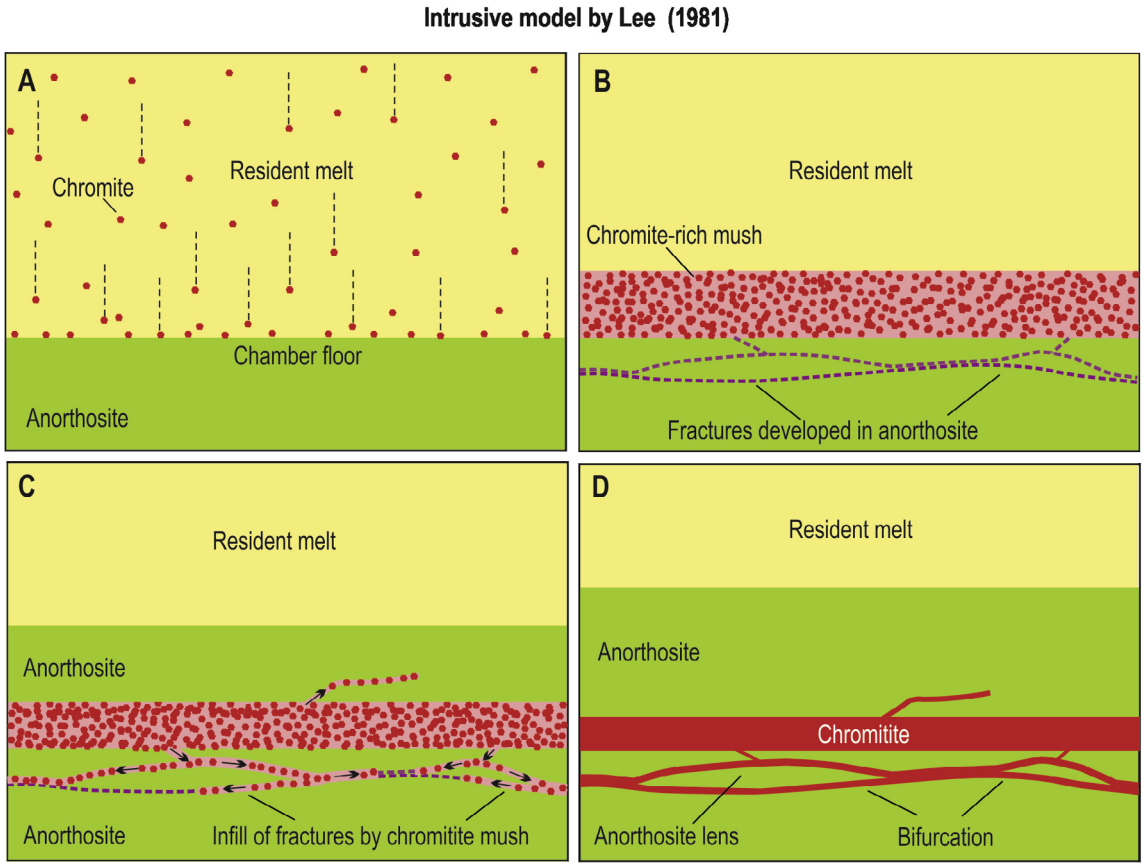

Fig. 24. A cartoon of the intrusive model proposed by Lee (1981) for the formation of chromitite layering and associated bifurcations. Gravitationally unstable chromite-rich mush on the chamber floor collapsed through fractures into the underlying cumulates. The anastomosing fractures separate the cumulates into lenses that control the distribution of the collapsing chromite mush. In addition, some chromite mush may also be sucked or squeezed upwards into fractures in the overlying anorthosite.

regional type erosion of the cumulate pile by flowing superheated melt. Both field observations (e.g. Swanson, 1973; Kauahikaua et al., 1998) and theoretical and experimental investigations (e.g. Kerr, 2001, 2009) show that the thermal erosion of the floor rocks by laminar flows of basaltic lavas is in the range of several centimetres per day. The second stage starts after the flooding of the entire chamber and mostly occurs via chemical erosion (dissolution) of footwall rocks, aided by vigorous convection within a basal layer of superheated magma. The rate of erosion at this stage is relatively slow but occurs over a time scale of several dozen years. Erosional processes in the second stage are therefore likely to be predominant.

It is possible to make some rough estimates of how much magma would be required during the second stage to cause the erosion observed and how long this process would take. The ratio of melt required to dissolve a given amount of cumulate (R = melt/-solid ratio) can be defined as:

$$R = (\rho_s L_s)/(\rho_l Cp \Delta T_s);$$

where ρ_s = density of the solid = 3.00 g/cm^3, L_s – latent heat of the solid = 300 J/g, ρ_l – density melt = 2.6 g/cm^3, Cp – heat capacity = 1.34 J/(g°C), ΔT_s – superheat = 10 °C. Note that in this equation (ρ_s L_s) is the heat needed to dissolve a given volume of solid whereas (ρ_l CpΔT_s) is the heat available in the magma for dissolution. Solving for the values given above yields the following results:

$$R = (3.0 \times 300)/(2.6 \times 1.34 \times 10) = 25.83$$

Thus to dissolve 1 m of cumulates one would need, at least, 1 × 25.83 = 25.83 m of melt that is superheated by 10 °C. The rate of dissolution in such a situation has been estimated by Kerr (1994) to be up to 10 cm/year. It would therefore take ~10 years to dissolve 1 m of floor cumulates by a 25.83 m thick column of magma superheated by 10 °C. Bearing in mind that the formation of a chromitite requires extraction of chromite from a large volume of melt (e.g. Campbell and Murck, 1993), the thickness of the convecting magma residing on the floor of the chamber could easily be more than 100 m, which would reduce the superheating required to less than 2.5 °C. The aim of these simple calculations is to show that removal of a substantial amount of footwall cumulate by melting and dissolution is possible, and can be achieved by a melt that is only slightly superheated relative to its liquidus temperature.

7.3. Cryptic layering, crystallization sequence and liquidus melt densities

The injection of superheated, more primitive, melt followed by thermochemical erosion of the chamber floor should be expected to be documented by reversals towards more magnesian orthopyroxene and anorthitic plagioclase. No compositional data are available from the DRL to confirm this prediction because sampling is not permitted at this protected locality. However, sparse microprobe data on orthopyroxene and plagioclase from the UG1 sequence in the Eastern Bushveld (Cameron, 1982, his Fig. 9) do not show the predicted changes in cumulus mineral compositions. The hypothesis requires testing by detailed study of cumulus mineral compositions through the UG1 sequence. Until this is carried out we would argue, however, that replenishment by superheated melt needs not necessarily result in reversals in mineral compositions.

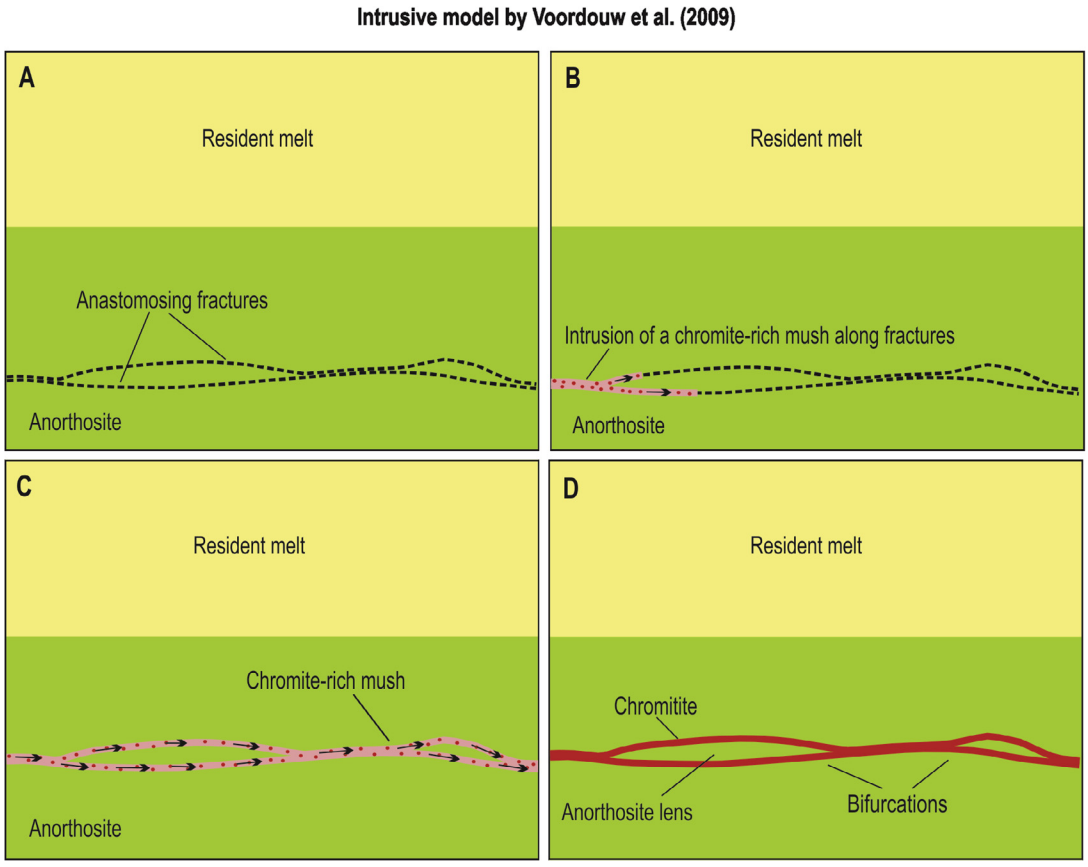

Fig. 25. The intrusive model formulated by Voordouw et al. (2009) for the formation of bifurcating chromitites appeals to anastomosing fractures in anorthositic cumulates that are later exploited by chromite-rich suspensions ascending from a deeper-seated magma chamber. See text for the discussion.

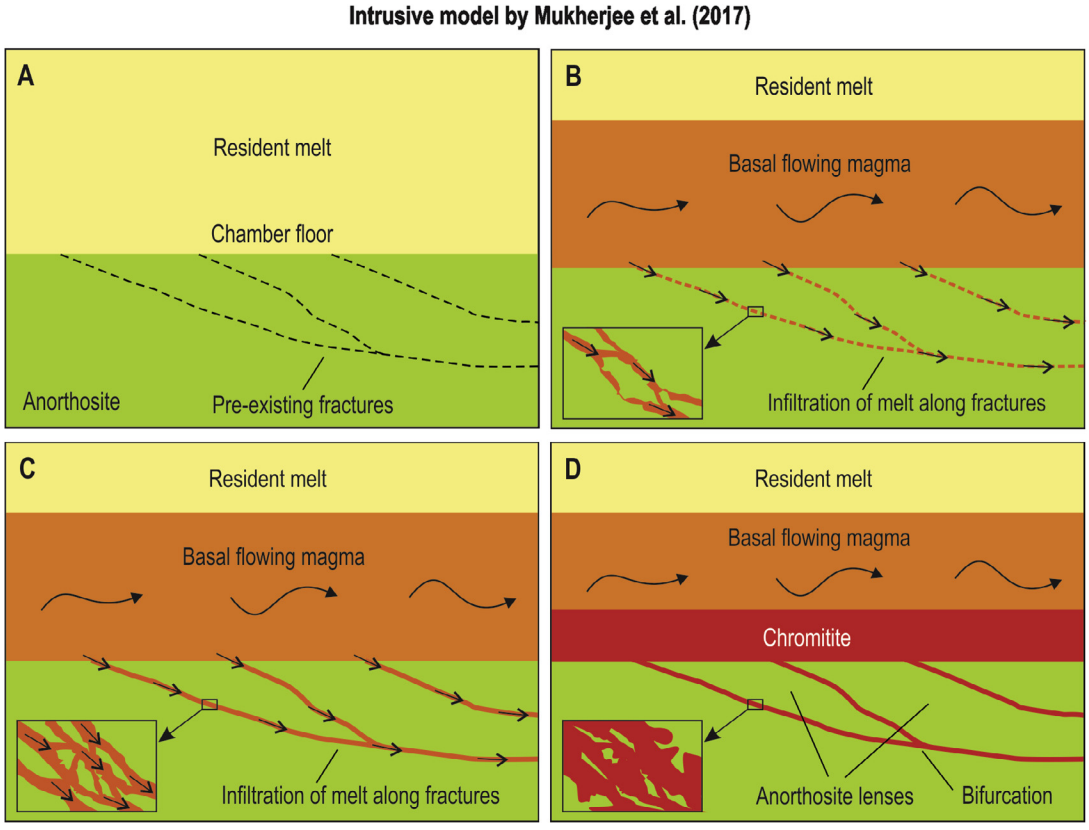

Fig. 26. An illustration of the intrusive model advanced by Mukherjee et al. (2017) for the formation of bifurcating chromitites. The anorthosite lenses responsible for the divergence of chromitite layers were supposed to have formed by anastomosing fractures in anorthositic cumulates that were later invaded by chromite-saturated melt. See text for the discussion.

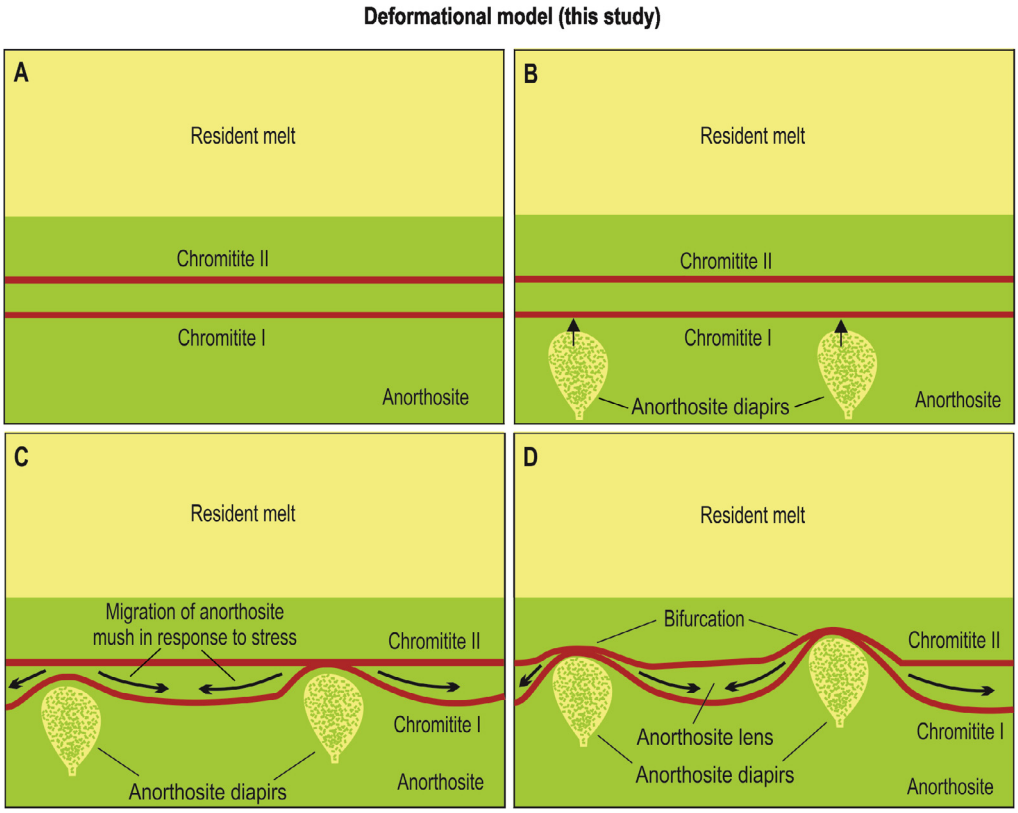

Fig. 27. A sketch of the deformational model for the formation of bifurcating chromitites proposed here. The central tenet is that the anorthosite lenses responsible for the divergence of chromitite layers were a result of the postcumulus redistribution of mobile plagioclase cumulate between chromitite layers in response to rising anorthosite diapirs. See text for the discussion.

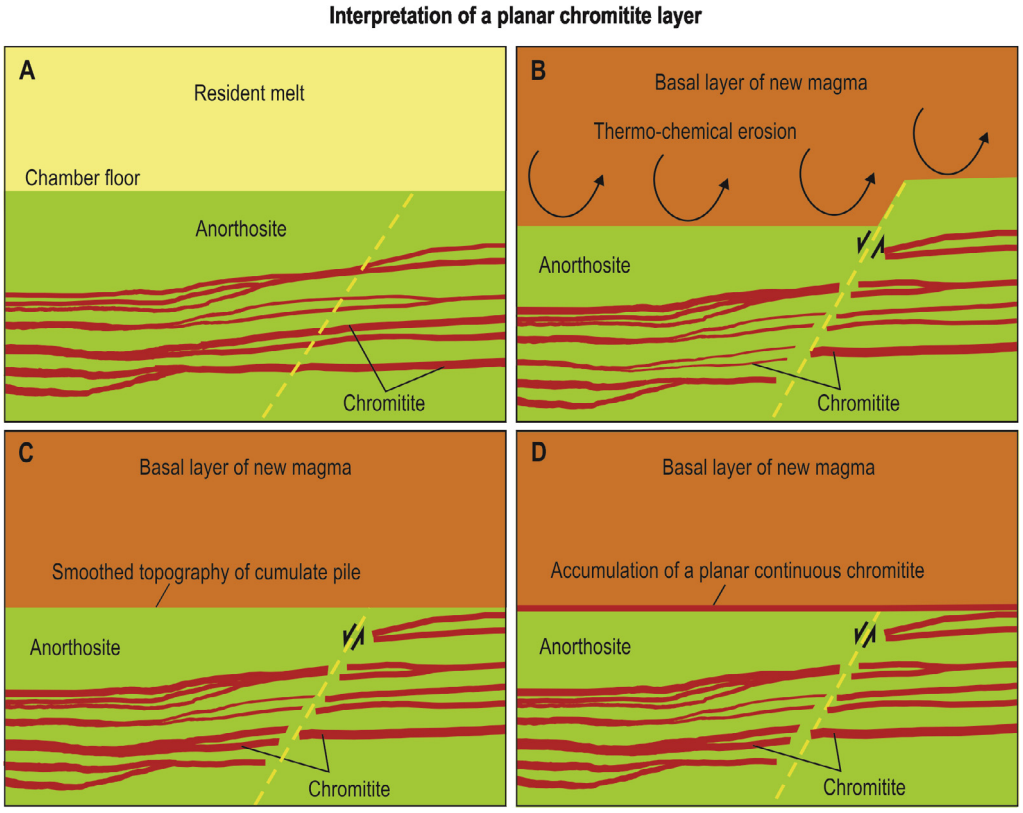

Fig. 28. The mechanism proposed here for the formation of disrupted chromitite layers overlain by non-deformed chromitite layers (based on Fig. 9A). The cumulates (A) containing multiple bifurcating chromitite layers are displaced along a normal fault (B). This results in the disruption of the chromitite layers and the formation of a step in the chamber floor. Subsequent thermo-chemical erosion smoothed out the irregularities on the chamber floor (C) so that the next chromitite seam was deposited on a flat surface (D). The relationships indicate active magmatic erosion of footwall rocks and chromitite formation directly on the chamber floor.

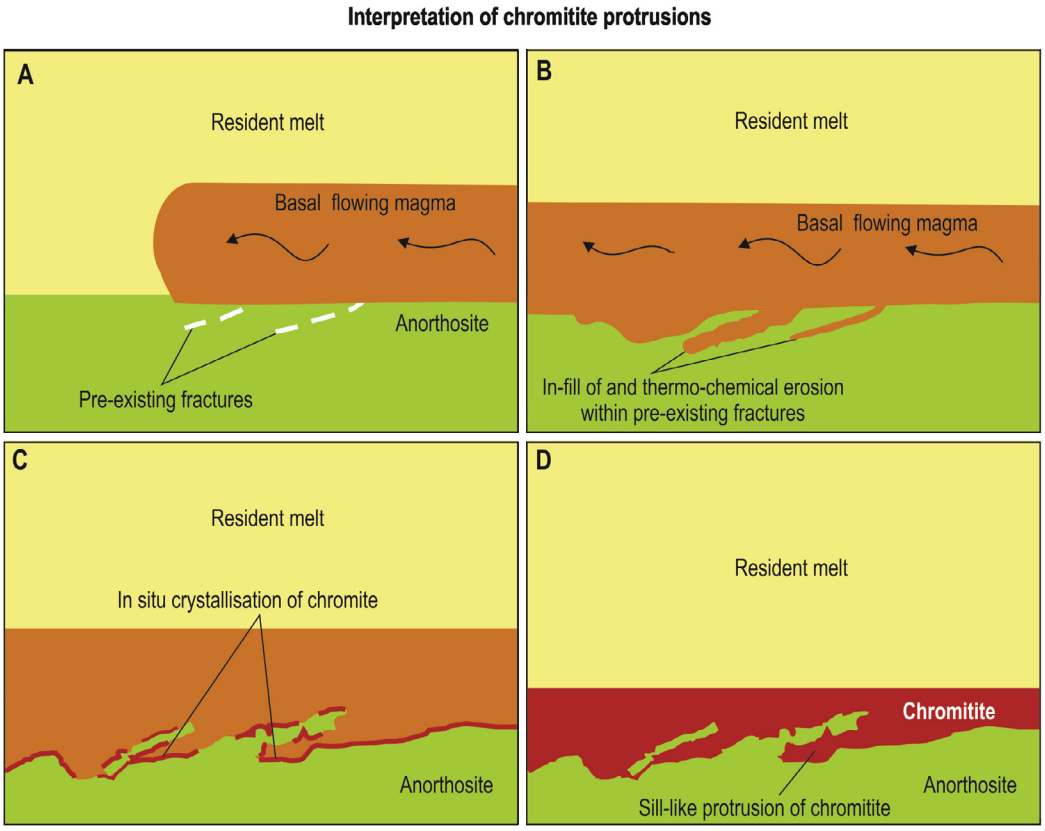

Fig. 29. A sketch of the events that led to the formation of sill-like protrusions of chromitite in footwall anorthosite. Dense magma flowing over anorthositic cumulates (A) intrudes into pre-existing fractures and erodes the footwall anorthosite (B). On cooling chromite starts crystallizing *in situ* (C) and drapes irregularities, including the sill-like cavities in the footwall anorthosites (D). Such relationships are indicative of the basal emplacement of the magma parental to chromitite, very reactive nature of this magma and the *in situ* crystallization of chromite beneath the screen.

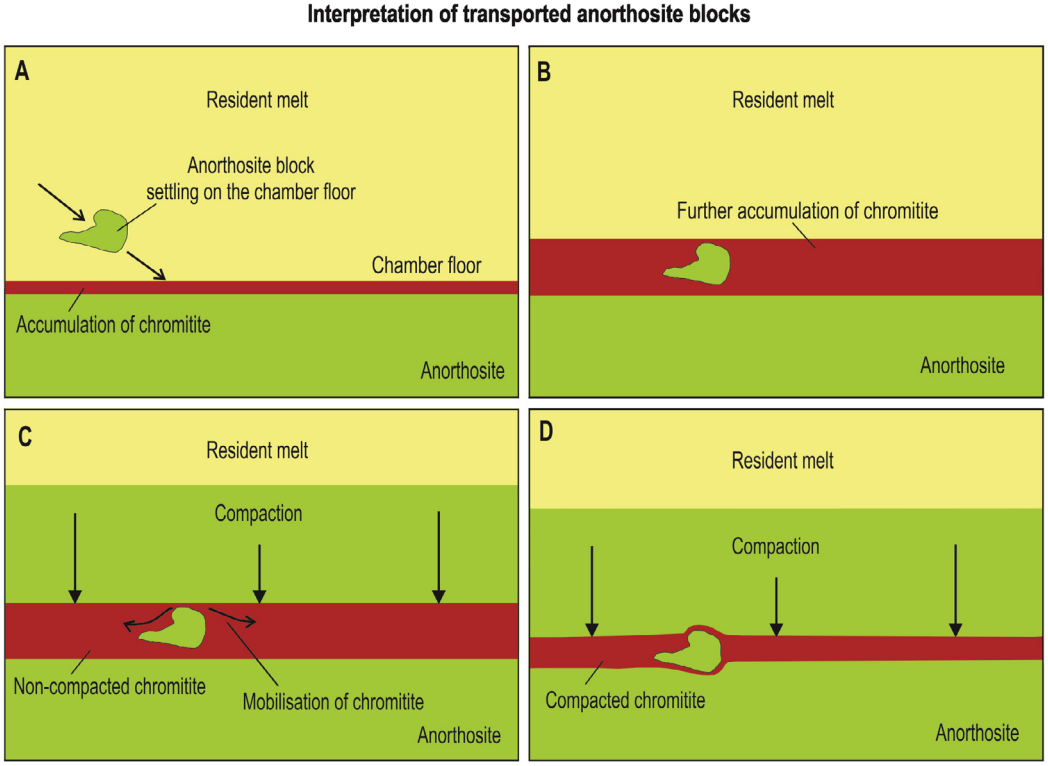

Fig. 30. A sketch of the emplacement of anorthosite blocks in chromitites. The magma in the chamber crystallizes chromite that is deposited on the chamber floor as a continuous layer. Anorthosite blocks settle onto the basal chromite mush (A) and subsequent crystallization of chromite covers them over (B). This is followed by crystallization of plagioclase-chromite cumulate and compaction of underlying layers. Chromite crystals in the chromitite layer are displaced away from the tops of the blocks (C). The chromitite layer eventually moulds to the shape of anorthosite blocks (D). The relationships of anorthosite blocks within chromitite are evidence for the formation of chromitite on the floor of the magma chamber.

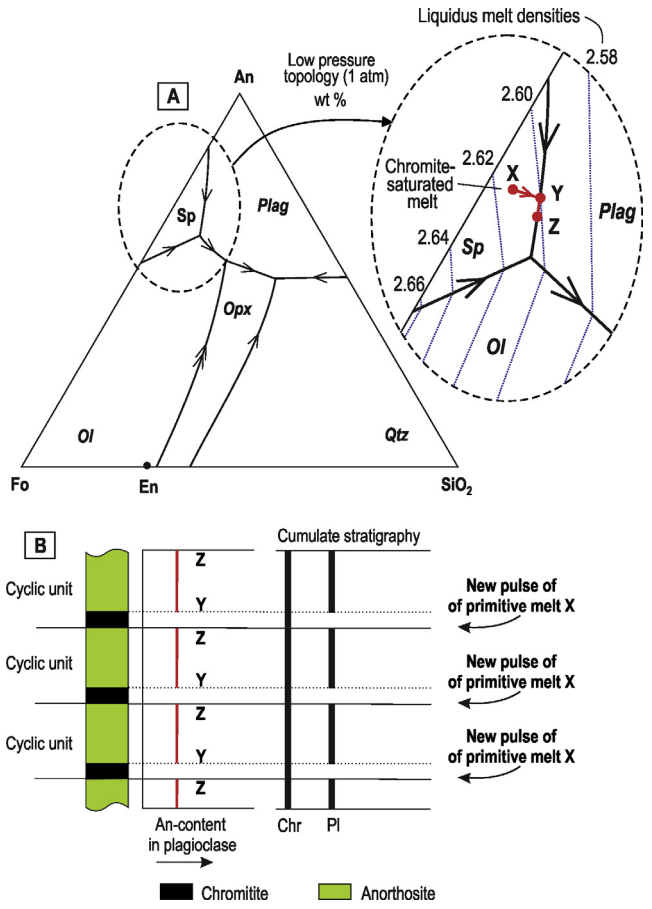

Fig. 31. The pseudoternary phase diagram Fo-An-SiO_2 (A) showing that replenishment of the magma chamber by the same primitive chromite-saturated melt X may produce a rock sequence consisting of multiple, chromitite-anorthosite cyclic units with limited cryptic variation in plagioclase composition (B). This is because each anorthosite layer starts crystallizing from a melt of virtually the same melt Y that experiences little fractionation before the subsequent replenishment event (A). Fo – forsterite, An – anorthite, En – enstatite, Sp – spinel, Qtz – quartz, Ol – olivine, Opx – orthopyroxene, Plag – plagioclase. Cotectic and reaction lines are indicated by one and two arrows, respectively. Phase diagram is simplified from Andersen (1915) and Irvine (1975). Liquidus melt densities (g/cm^3) in an insert (A) are from Irvine et al. (1983, their Fig. 6A).

This idea is illustrated using a pseudoternary system Fo-An-SiO_2 (Fig. 31). We suggest considering the UG1 sequence at the DRL as consisting of several chromitite-anorthosite cyclic units, with each being produced from a separate pulse of similar melt (X) located in the stability field of spinel (chromite). Each pulse is supposed to be emplaced as a basal flow with little mixing with the resident melt taking place. An inferred crystallization sequence (Fig. 31A) of each pulse is chromite (along the path from X to Y) followed by chromite and plagioclase (along the path from Y to Z). No detectable change in plagioclase composition is expected within anorthosite if one assumes that the path Y-Z constitutes only a small amount (say, less than 1%) of fractional crystallization of the melt. Under these assumptions the composition of plagioclase in the whole sequence would remain much the same because each anorthosite will start crystallizing from the melt of similar composition Y (Fig. 31B). The scenario illustrates the possibility that a lack of significant changes in plagioclase composition at the boundaries of cyclic units, as appears to be the case at the DRL, should not be taken as evidence against the injection of primitive magma into the evolving chamber.

To be emplaced as a basal flow, each new pulse of parental liquid must be denser than the resident melt in the chamber. This appears to be consistent with liquidus melt densities in the system in question (Fig. 31A, insert). Spinel fractionation along the path from X to Y may result in a strong decrease in liquid density that is not compensated by the subsequent slight increase in the density associated with crystallization of plagioclase (along the path from Y to Z). This means that the new replenishing melt X will be denser than the resident liquid Z and it will form a basal flow, an inference that is fully consistent with field relationships indicating intensive erosion of floor cumulates by new magma pulses (Figs. 5 and 11).

7.4. An erosional model for bifurcating chromitite layers

The most important inference from the field relationships as presented here is that magmatic erosion has played a crucial role in the petrogenesis of UG1 chromitite-anorthosite sequence. On this basis we introduce a novel 'erosional' model for the formation of chromitite bifurcations (Fig. 32). This model involves the emplacement of a basal flow of dense and superheated magma into the chamber over pre-existing anorthosite cumulates. After a period of thermo-chemical erosion of the floor cumulates and related cooling of the magma, it crystallized a chromitite layer *in situ*, which draped over the irregularities of the erosional surface (Fig. 32A). With further cooling the magma reached saturation in plagioclase and crystallized a continuous layer of plagioclase-chromite cumulate that covered the underlying chromitite (Fig. 32B). This was followed by the emplacement of a new basal flow of superheated magma that initiated a new cycle of thermo-chemical erosion of the floor cumulates. The extent of the erosion was variable and locally lenses of anorthosite (more resistant to erosion) remained resting on a chromitite layer. The erosion was commonly arrested at a chromitite layer (Fig. 32C) because it was either too refractory to be eroded, or its dissolution produced a thin liquid boundary layer, which was denser than the overlying melt in the chamber. Such a basal layer cannot be normally removed by convection and it may therefore completely terminate the erosion (e.g. Campbell, 1986). On cooling, the magma crystallized a new layer of chromitite that draped over the remnant anorthosite lenses and exhumed parts of the previously formed chromitite layer (Fig. 32D). This led to locally converging and diverging of chromitite layers along strike, i.e. bifurcation with chromitite layers that bridge different stratigraphic horizons in the cumulate sequence. Not all anorthosites were formed from magmas that were derived from those that initially crystallized chromitites. Some anorthosites appear to have crystallized from independent pulses of superheated magma that locally caused erosion of previously deposited chromitite. This would explain lobate contacts of some chromitites with the overlying anorthosites. This sequence of events was accompanied by several additional processes, such as intrusion of magma into footwall anorthosite to form sill-like chromitite protrusions (Figs. 27 and 29); lateral transport of anorthosite blocks and their encapsulation in chromitite (Fig. 30); disruption and displacement of the cumulates with attendant resetting of the floor topography by erosion and deposition of planar and non-deformed chromitite layers (Fig. 28); ductile and brittle deformation of igneous layering, especially at the margins of rising anorthosite diapirs (Fig. 27). The repetition of magma emplacement and erosion resulted in a complex package of multiply-bifurcating and locally disrupted chromitite layers separated by anorthosite lenses (Fig. 3). After deformation, oikocrysts of orthopyroxene crystallized from melt trapped in anorthosites (Fig. 19) and oikocrysts of plagioclase crystallized in chromitite (Fig. 20). The interstitial plagioclase in chromitite locally grew from adjacent cumulus plagioclase crystals forming almost continuous rims along layer boundaries (Fig. 20C, D) because self-nucleation on pre-existing crystals of the same mineral is the most kinetically favourable process (e.g. Campbell, 1996).

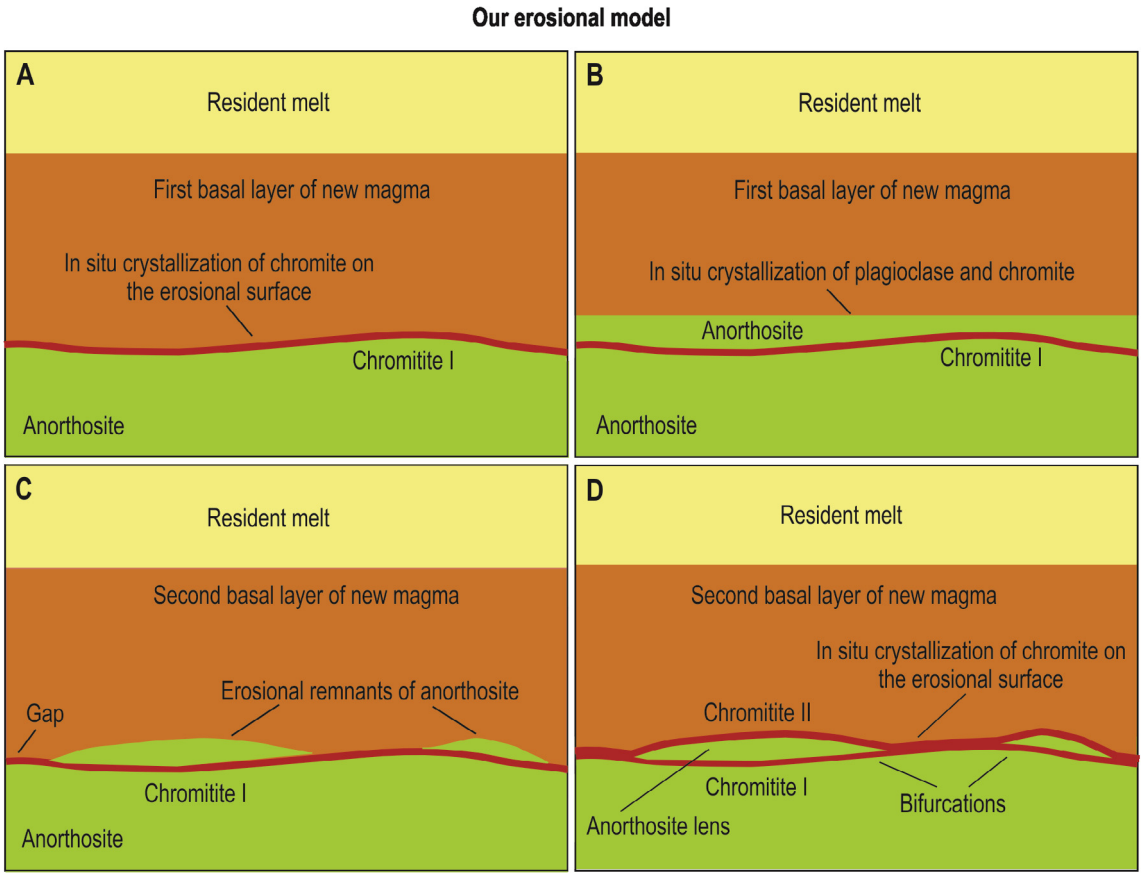

Fig. 32. An illustration of our erosional model for the formation of bifurcating chromitites. The crucial feature of this model is that the anorthosite lenses responsible for the splitting of chromitite layers are the result of patchy thermochemical erosion of plagioclase cumulate on the chamber floor by pulses of new, dense and superheated magma. See text for the discussion.

8. Conclusions

One unexpected outcome of this study is the recognition that bifurcation of UG1 chromitite layers is the result of several distinctly different processes. The combination of these processes resulted in morphologically distinct types of bifurcation that has hampered attempts to decipher the origin of this phenomenon. Based on the observations presented here, we argue that the principal type of UG1 chromitite bifurcation (Fig. 3) is a syn-magmatic feature, which formed on the floor of the Bushveld magma chamber in response to replenishment of the chamber by pulses of dense, slightly superheated magma. Features such as: lobate contacts between chromitite and anorthosite; gaps and abrupt termination of anorthosite layers within chromitites; anorthosite inclusions and their irregular margins; sill-like protrusions of chromitite in footwall anorthosite; and disrupted portions of the cumulate pile overlain by planar, non-deformed chromite layers are interpreted as evidence for intense erosion of footwall rocks by replenishing, superheated magmas. We suggest that magmatic erosion is primarily responsible for the origin of the principal type of bifurcating chromitite layers. Most lenses of anorthosite – the principal cause of chromitite bifurcation – are erosional remnants of previously continuous layers of anorthosite (Fig. 32).

The predominant type of chromitite bifurcation appears to be complicated by the presence of, at least, three subordinate types that are the result of other processes. One subtype includes chromitite protrusions (Fig. 10) some of which contain *in situ* inclusions of footwall anorthosite (Fig. 11A). This is attributed to the crystallization of chromite-saturated melt moving through fractures in the footwall cumulates (Fig. 26). Another subtype is associated with thin offshoots of chromitite that branch from thicker chromitite layers at high angles and abruptly terminate in adjacent anorthosite over distances of a few centimetres to decimetres (Figs. 17 and 18). These are interpreted as the result of late-stage mobilisation of chromite-rich mush and its intrusion into footwall and hanging-wall anorthosite along fractures developed in the cumulates (Fig. 24). A third subtype comprises merging of chromitite layers at the margins of anorthosite domes (Fig. 13). This is explained as the result of plastic deformation of semi-consolidated cumulates due to the rise of anorthosite diapirs (Fig. 27). All these three subtypes of chromitite bifurcations are morphologically distinct and should not be normally confused with the principal type of chromitite bifurcation (Fig. 3). Interestingly, our pilot study of the UG1 layering at the Impala and Rustenburg Platinum Mines, Eastern Bushveld indicates that there are some additional subtypes of bifurcating chromitite layers that are absent from the DRL. These subtypes are waiting to be properly documented and interpreted.

The present study indicates that magmatic erosion is an important agent that can result in significant modification of igneous layering. Magmatic erosion can be responsible for enigmatic features of some igneous layering, such as bifurcating chromitite layers that unexpectedly bridge different stratigraphic horizons in plagioclase cumulates. We suggest erosion should be included in a list of conventional processes that are thought to be responsible for the origin of layer boundaries in mafic-ultramafic layered intrusions (Naslund and McBirney, 1996; Namur et al., 2015).

Acknowledgements

This work is based on the first author's honours research project that was supported by the National Research Foundation (NRF) of South Africa in the form of Research Grants 87677, 90834 and 91812 to Rais Latypov. Any opinion, finding and conclusion or recommendation expressed in this material is that of the authors and the NRF does not accept any liability in this regard. The hypothesis of the erosional nature of UG1 chromitite bifurcations has emerged from a lively discussion with Richard Hornsey during our field visit to the DRL. We are grateful to Sofya Chistyakova, Grant Cawthorn, Paul Nex, Richard Hornsey, Ria Mukherjee and Emma Hunt for fruitful discussions on many aspects of this study. They bear, however, no responsibility for the conclusions we have reached. Sofya Chistyakova is also greatly thanked for assistance with field work and preparation of figures. We thank Emma Hunt for editing and comments that have improved an early version of the manuscript. The official reviews by Ed Mathez, Wolf Maier and Tony Morse and editorial handling by Sisir Mondal are highly acknowledged. We are especially grateful to Brian Robins for his meticulous editing, comments and questions that have significantly improved the final version of the manuscript.

Appendix A. Supplementary data

Supplementary data associated with this article can be found, in the online version, at http://dx.doi.org/10.1016/j.oregeorev.2017.02.026. These data include GPS coordinates of the most important outcrops described in this article.

References

Andersen, O., 1915. The system anorthite-forsterite-silica. Am. J. Sci. 39, 407–454.
Cameron, E.N., 1963. Structure and rock sequence of the critical zone of the Eastern Bushveld Complex. Mineral. Soc. Am., Special Paper 1, 93–107.
Cameron, E.N., 1964. Chromite deposits of the eastern part of the Bushveld Complex. In: Haughton, S.H. (Ed.), The geology of some ore deposits in Southern Africa, 2. Special Publication Geological Society of South Africa, pp. 131–168.
Cameron, E.N., 1978. The lower zone of the eastern Bushveld Complex in the Oliphants river trough. J. Petrol. 19, 437–462.
Cameron, E.N., 1982. The upper critical zone of the eastern Bushveld Complex; precursor of the Merensky Reef. Econ. Geol. 77, 1307–1327.
Campbell, I.H., 1986. A fluid dynamic model for potholes of the Merensky Reef. Econ. Geol. 81, 1118–1125.
Campbell, I.H., 1996. Fluid dynamic processes in basaltic magma chambers. In: Cawthorn, R.G. (Ed.), Layered Intrusions. Developments in Petrology, 15. Elsevier, pp. 45–76.
Campbell, I.H., Murck, B.W., 1993. Petrology of the G and H chromitite zones in the Mountain View area of the Stillwater Complex, Montana. J. Petrol. 34, 291–316.
Cawthorn, G., 2003. Genesis of magmatic oxide deposits – a view from the Bushveld Complex. Norges geologiske undersokelse Special Publication 9, 11–21.
Cawthorn, R.G., 2015. Bushveld Complex. In: Charlier, B., Namur, O., Latypov, R., Tegner, C. (Eds.), Layered Intrusions. 1st ed. Springer, pp. 517–587. Weteringschans: Springer International Publishing. New York City: Springer.
Cawthorn, R.G., Walraven, F., 1998. Emplacement and crystallization time for the Bushveld Complex. J. Petrol. 39, 1669–1687.
Cawthorn, R.G., Barnes, S.J., Ballhaus, C., Malitch, K.N., 2005. Platinum-group element, chromium, and vanadium deposits in mafic and ultramafic rocks. Econ. Geol., 215–249 100th Anniversary Volume.
Cousins, C.A., Feringa, G., 1964. The chromite deposits of the western belt of the Bushveld Complex. In: Haughton, S.H. (Ed.), The geology of some ore deposits in southern Africa, 2. Special Publication Geological Society of South Africa, pp. 183–202.
De Klerk, W.J., 1992. Petrogenesis of the Upper Critical Zone of the Western Bushveld Complex with emphasis on the UG1 footwall and Bastard Units (Ph.D. thesis). Rhodes University, Grahamstown, p. 294.
Eales, H.V., Cawthorn, R.G., 1996. The Bushveld Complex. In: Cawthorn, R.G. (Ed.), Layered intrusions. Elsevier, Amsterdam. 531 Develop. Petrol. 15.
Eales, H.V., Costin, G., 2012. Crustally contaminated komatiite: primary source of the chromitites and Marginal, Lower, and Critical zone magmas in a staging chamber beneath the Bushveld Complex. Econ. Geol. 107, 645–665.
Eales, H.V., Field, M., De Klerk, W.J., Scoon, R.N., 1988. Regional trends of chemical variation and thermal erosion in the Upper Critical Zone, Western Bushveld Complex. Mineral. Mag. 52, 63–79.
Ferguson, J., Botha, E., 1963. Some aspects of igneous layering in the basic zones of the Bushveld Complex. Trans. Geol. Soc. South Africa 66, 259–278.
Finn, C.A., Bedrosian, P.A., Cole, J.C., Khoza, T.D., Webb, S.J., 2015. Mapping the 3D extent of the Northern Lobe of the Bushveld layered mafic intrusion from geophysical data. Precambr. Res. 268, 279–294.
Gain, S.B., 1985. The geologic setting of the platiniferous UG2 chromitite layer on the farm Maandagshoek, Eastern Bushveld Complex. Econ. Geol. 80, 925–943.
Hall, A.L. (Ed.), 1932. The Bushveld Igenous Complex in central Transvaal, 28. Geological Society of South Africa Memoir, p. 544.
Hatton, C.J., von Gruenewaldt, G., 1987. The geological setting and petrogenesis of the Bushveld chromitite layers. In: Stowe, C.W. (Ed.), Evolution of Chromium Ore Fields. Van Nostrand, New York, pp. 109–143.
Hess, H.H., 1960. Stillwater igneous complex, Montana – a quantitative mineralogical study. Geol. Soc. Am. Mem. 80, 230.
Irvine, T.N., 1975. Olivine-pyroxene-plagioclase relations in the system Mg_2SiO_4 - $CaAl_2Si_20_8$-$KAlSi_3O_8$-SiO_2 and their bearing on the differentiation of stratiform intrusions. Carnegie Inst. Washington 74, 492–500.
Irvine, T.N., Keith, D.W., Todd, S.G., 1983. The J-M platinum–palladium reef of the Stillwater Complex, Montana II: origin by double-diffusive convective magma mixing and implications for the Bushveld Complex. Econ. Geol. 78, 1287–1334.
Kauahikaua, J., Cashman, K.V., Mattox, T.N., Heliker, C.C., Hon, K.A., Mangan, M.T., Thornber, C.R., 1998. Observations on basaltic lava streams in tubes from Kilauea Volcano, Island of Hawai'i. J. Geophys. Res. 103, 27,303–27,323.
Kerr, R.C., 1994. Dissolving driven by vigorous compositional convection. J. Fluid Mech. 280, 287–302.
Kerr, R.C., 2001. Thermal erosion by laminar lava flows. J. Geophys. Res. 106, 26453–26465.
Kerr, R.C., 2009. Thermal erosion of felsic ground by the laminar flow of a basaltic lava, with application to the Cave Basalt, Mount St. Helens, Washington. J. Geophys. Res. 114 (B09204), 1–14.
Kinnaird, J.A., Kruger, F.J., Nex, P.A.M., Cawthorn, R.G., 2002. Chromite formation – a key to understanding processes of platinum enrichment. Trans. Inst. Min. Metall. 111, B23–B35.
Kruger, F.J., Marsh, J.S., 1985. The mineralogy, petrology and origin of the Merensky cyclic unit in the western Bushveld Complex. Econ. Geol. 80, 958–974.
Latypov, R.M., Chistyakova, S.Yu., Page, A., Hornsey, R., 2015. Field evidence for the *in situ* crystallization of the Merensky Reef. J. Petrol. 56, 2341–2372.
Latypov, R.M., Chistyakova, S.Yu., Barnes, S.J., Hunt, E.J., 2017. Origin of platinum deposits in layered intrusions by in situ crystallization: evidence from undercutting Merensky Reef of the Bushveld Complex. J. Petrol. (accepted manuscript)
Lee, C.A., 1981. Post-deposition structures in the Bushveld Complex mafic sequence. J. Geol. Soc., London 138, 327–341.
Maier, W.D., Barnes, S.J., 1999. Platinum-group elements in silicate rocks of the Lower, Critical, Main Zones at Union Section, Western Bushveld Complex. J. Petrol. 40, 1647–1671.
Maier, W., Barnes, S., 2008. Platinum-group elements in the UG1 and UG2 chromitites, and the Bastard reef, at Impala platinum mine, western Bushveld Complex, South Africa: evidence for late magmatic cumulate instability and reef constitution. S. Afr. J. Geol. 111, 159–176.
Maier, W.D., Eales, H.V., 1997. Correlation within the UG2–Merensky Reef interval of the Western Bushveld Complex, based on geochemical, mineralogical and petrological data. Geol. Surv. South Africa Bull. 120, 56.
Maier, W.D., Barnes, S.-J., Groves, D.I., 2013. The Bushveld Complex, South Africa: formation of platinum–palladium, chrome- and vanadium-rich layers via hydrodynamic sorting of a mobilized cumulate slurry in a large, relatively slowly cooling, subsiding magma chamber. Miner. Deposita 48, 1–56.
Mondal, S.K., Mathez, E.A., 2007. Origin of the UG2 chromitite layer, Bushveld Complex. J. Petrol. 48, 495–510.
Mukherjee, R., Latypov, R., Balakrishnan, A., 2017. An intrusive origin of some massive chromitite layers: insights from field relationships at the Impala Platinum Mine, Bushveld Igneous Complex. Ore Geol. Rev. (accepted manuscript)
Naldrett, A.J., Wilson, A., Kinnaird, J., Chunnett, G., 2009. PGE tenor and metal ratios within and below the Merensky Reef, Bushveld Complex: implications for its genesis. J. Petrol. 50, 625–659.
Naldrett, A., Kinnaird, J., Wilson, A., Yudovskaya, M., Chunnett, G., 2011. Genesis of the PGE-enriched Merensky Reef and chromitite seams of the Bushveld Complex. In: Li, C., Ripley, E.M. (Eds.), Review in economic geology: magmatic Ni-Cu and PGE deposits: geology, geochemistry and genesis, 17, pp. 235–296.
Naldrett, A.J., Wilson, A., Kinnaird, J., Yudovskaya, M., Chunnett, G., 2012. The origin of chromitites and related PGE mineralization in the Bushveld Complex: new mineralogical and petrological constraints. Miner. Deposita 47, 209–239.
Namur, O., Abily, B., Boudreau, A.E., Blanchette, F., Bush, J.W.M., Ceuleneer, G., Charlier, B., Donaldson, C.H., Duchesne, J., Higgins, M.D., Morata, D., Troels, Nielsen, F.D., O'Driscoll, B., Pang, K.N., Peacock, T., Spandler, C.J., Toramaru, A., Veksler, I.V., 2015. Igneous layering in basaltic magmas. In: Charlier, B., Namur, O., Latypov, R., Tegner, C. (Eds.), Layered Intrusions. first ed. Springer, pp. 75–152. Weteringschans: Springer International Publishing. New York City: Springer.
Naslund, H.R., McBirney, A.R., 1996. Mechanisms of formation of igneous layering. Dev. Petrol. 15, 1–43.
Nex, P.A.M., 2004. Formation of bifurcating chromitite layers if the UG1 in the Bushveld Igneous Complex, an analogy with sand volcanoes. J. Geol. Soc., London 161, 903–909.

Roberts, M.D., Reid, D.L., Miller, J.A., Basson, I.J., Roberts, M., Smith, D., 2007. The Merensky Cyclic Unit and its impact on footwall cumulates below Normal and Regional Pothole reef types in the Western Bushveld Complex. Miner. Deposita 42, 271–292.
Roeder, P.L., Gofton, E., Thornber, C., 2006. Cotectic proportions of olivine and spinel in olivine-tholeiitic basalt and evaluation of pre-eruptive processes. J. Petrol. 47, 883–900.
Sampson, E., 1932. Magmatic chromite deposits in Southern Africa. Econ. Geol. 27, 113–144.
Schürmann, L.W., Grabe, P.-J., Steenkamp, C.J., 1998. In: Wilson, M.G.C., Anhaeussern, C.R. (Eds.), The mineral resources of South Africa, 16. Council for Geoscience Handbook, p. 740.
Scoon, R.N., Teigler, B., 1994. Platinum-group element mineralization in the critical zone of the Western Bushveld Complex: I sulfide-poor chromitites below the UG2. Econ. Geol. 89, 1094–1121.
Smith, D.S., Basson, I.J., Reid, D.L., 2003. Normal reef sub-facies of the Merensky Reef at Northam Platinum Mine, Zwartklip facies, Western Bushveld Complex, South Africa. Can. Mineral. 42, 243–260.
Swanson, D.A., 1973. Pahoehoe flows from the 1969–1971 Mauna Ulu eruption, Kilauea Volcano, Hawaii. Geol. Soc. Am. Bull. 84, 615–626.
Teigler, B., Eales, H.V., 1996. The lower and critical zones of the western limb of the Bushveld Complex, as indicated by the Nooitgedacht boreholes. Geol. Surv. South Africa Bull. 111, 126.
Van Biljon, S., 1963. Structures in the basic belt of the Bushveld Complex. Trans. Geol. Soc. South Africa 66, 11–47.
Vermaak, C.F., 1976. The Merensky Reef – thoughts on its environment and genesis. Econ. Geol. 71, 1270–1298.
Viring, R.G., Cowell, M.W., 1999. The Merensky Reef on Northam Platinum Limited. S. Afr. J. Geol. 102, 192–208.
Voordouw, R., Gutzmer, J., Beukes, N.J., 2009. Intrusive origin for Upper Group (UG1, UG2) stratiform chromitite seams in the Dwars River area, Bushveld Complex, South Africa. Mineral. Petrol. 97, 75–94.
Wager, L.R., Brown, G.M., 1967. Layered Igneous Rocks. Edinburgh and London, Oliver and Boyd, p. 588.
Webb, S.J., 2009. The use of potential field and seismological data to analyze the structure of the lithosphere beneath southern Africa (PhD thesis). University of Witwatersrand, p. 337.
Zeh, A., Ovtcharova, M., Wilson, A.H., Shaltegger, U., 2015. The Bushveld Complex was emplaced and cooled in less than 1 million years – results of zirconology, and geotectonic implications. Earth Planet. Sci. Lett. 418, 103–114.